REVIEW ARTICLE

Molecular Junction Photocatalysts in Graphitic Carbon Nitride: Precise Characterization of Built-in Electric Fields and Challenges in Spatial Charge Separation

Kaichi Chen[1], **Zhicheng Zheng**[1], **Yukun Fang**[1], **Yuanyuan Liu**[2,*] **and Xinli Guo**[1,*]

[1] State Key Laboratory of Engineering Materials for Major Infrastructure, School of Materials Science and Engineering, Southeast University, Nanjing 211189, China
[2] School of Chemistry and Chemical Engineering, Xuzhou University of Technology, Xuzhou 221018, China

Abstract

Graphitic carbon nitride ($g\text{-}C_3N_4$) has garnered interest as a versatile photocatalytic platform owing to its tailorable electronic architecture; however, its solar-to-chemical conversion is bottlenecked by high exciton binding energies and slow charge-carrier transport. To circumvent these impediments, the construction of "molecular junctions" within the conjugated polymeric scaffold enables atomically precise modulation of spatial electron configurations. Unlike conventional heterostructures relying on physical contact, molecular junctions employ robust covalent bridging, facilitating molecular orbital hybridization and π-conjugation. This review summarizes recent advances in molecular-junction-functionalized $g\text{-}C_3N_4$ photocatalysts, focusing on built-in electric field (BIEF) induction and its effects on charge-carrier dynamics. Molecular junctions are categorized into homojunctions exploiting structural polymorphisms and heterojunctions incorporating donor–acceptor moieties or single-atom sites. Structural asymmetry engenders steep potential gradients, mitigating exciton binding and promoting unidirectional charge migration. State-of-the-art BIEF characterization techniques—including Kelvin probe force microscopy (KPFM), density functional theory (DFT), and ultrafast transient absorption spectroscopy—are systematically examined. Finally, the catalytic efficacy of these molecular junction paradigms is assessed across solar-driven applications, including photocatalytic hydrogen evolution, overall water splitting, and hydrogen peroxide synthesis. The review concludes by outlining key bottlenecks and future directions, emphasizing atomically precise synthesis and operando characterization.

Keywords: graphitic carbon nitride, molecular junction, photocatalysis, built-in electric field, spatial charge separation.

Submitted: 09 March 2026
Accepted: 27 March 2026
Published: 03 April 2026

Vol. 2, **No.** 2, 2026.
10.62762/JAMR.2026.848022

***Corresponding authors:**
✉ Yuanyuan Liu
liuyuanyuan@xzit.edu.cn
✉ Xinli Guo
guo.xinli@seu.edu.cn

Citation
Chen, K., Zheng, Z., Fang, Y., Liu, Y., & Guo, X. (2026). Molecular Junction Photocatalysts in Graphitic Carbon Nitride: Precise Characterization of Built-in Electric Fields and Challenges in Spatial Charge Separation. *Journal of Advanced Materials Research*, 2(2), 119–141.

1 Introduction

In response to the escalating global energy crisis and environmental degradation, major economies have implemented "carbon peak and carbon neutrality" strategies as pivotal policy frameworks. Within this context, solar energy has emerged as a cornerstone of clean energy transition due to its inherent advantages of near-limitless abundance and renewability [1]. Photocatalytic technology, serving as a critical solar energy conversion pathway, demonstrates significant potential across energy production and environmental remediation applications. However, its practical implementation faces substantial challenges [2, 3], primarily originating from rapid photogenerated charge recombination and unsatisfactory quantum efficiency, which represent fundamental bottlenecks requiring urgent resolution. Graphitic carbon nitride (g-C_3N_4), as an emerging photocatalytic material, has garnered extensive attention in multiple photocatalytic applications owing to its moderate bandgap (2.7 eV) and excellent physicochemical stability [4–8]. However, its catalytic efficiency is fundamentally constrained by intrinsic limitations, including low specific surface area and rapid charge recombination. At the microstructural level, the highly symmetric configuration of g-C_3N_4 results in excessively uniform electron distribution, which impedes effective separation of photogenerated carriers. Currently, the construction of BIEF is regarded as a promising strategy to disrupt this charge equilibrium and enhance carrier separation efficiency.

In conventional research paradigms, heterojunction construction has been the most prevalent approach for inducing BIEF [9, 10]. This strategy exploits the Fermi level disparity between dissimilar semiconductor components to generate space-charge regions at contact interfaces, thereby facilitating charge migration [11, 12]. However, the efficacy of conventional heterojunctions is critically dependent on the quality of physical contact between phases. Such "face-to-face" [13] or "point-to-face" [14] contact interfaces based on physical stacking are inevitably accompanied by high-density electron trap states and substantial interfacial resistance, resulting in severe scattering losses during charge transfer across energy barriers. More critically, BIEF induced by conventional heterojunctions are typically confined to nanoscale interfacial regions, exhibiting limited capability to modulate bulk carrier dynamics within semiconductor components. This spatial localization effect fundamentally restricts the operational efficiency of traditional heterojunctions from reaching theoretical predictions. Consequently, there exists an urgent research imperative to explore molecular-level engineering of BIEF, aiming to achieve omnidirectional charge manipulation throughout the entire material architecture.

In contrast to conventional physical overlapping strategies, molecular junction engineering employs covalent grafting techniques to precisely anchor functional monomers as "electron pumps" or "charge-transfer mediators" at the periphery of g-C_3N_4 frameworks via robust chemical bonds (e.g., C-N, C=N, or C-C linkages). This atomic-scale linkage strategy achieves a paradigm shift from macroscopic interfacial transport to microscopic molecular orbital overlap, enabling direct symmetry breaking of intramolecular charge distribution that generates a robust directional electric field penetrating the entire framework, as illustrated in Figure 1. Such molecular-level BIEF not only effectively reduce exciton binding energies but also facilitate lossless ultrafast charge transfer from the polymeric matrix to active catalytic centers. Notwithstanding these advances, the precise construction of molecular-junction g-C_3N_4, their multiscale characterization, and the elucidation of their performance evolution mechanisms remain formidable challenges at the forefront of catalytic science. In particular, the dual-dimensional (qualitative-quantitative) profiling of BIEF not only constitutes an indispensable diagnostic criterion for successful material synthesis, but more fundamentally provides decisive mechanistic evidence that bridges the knowledge gap between atomic-scale structural motifs and macroscopic catalytic superiority. Currently, the academic community has developed various methodologies, including in situ experimental characterization and theoretical computational simulations, to probe BIEF. However, it is regrettable that there remains a lack of systematic reviews comprehensively elucidating the characterization logic and analytical processes of BIEF. In light of this, this paper will delve into the characterization framework of BIEF in molecular junction g-C_3N_4 from the perspective of their physical essence, aiming to provide systematic theoretical guidance and references for the rational design of photocatalytic materials and in-depth mechanistic exploration. Figure 2 illustrates the evolution of g-C_3N_4 based molecular junctions over the past decade. Given their unparalleled merits, a comprehensive review of current advancements

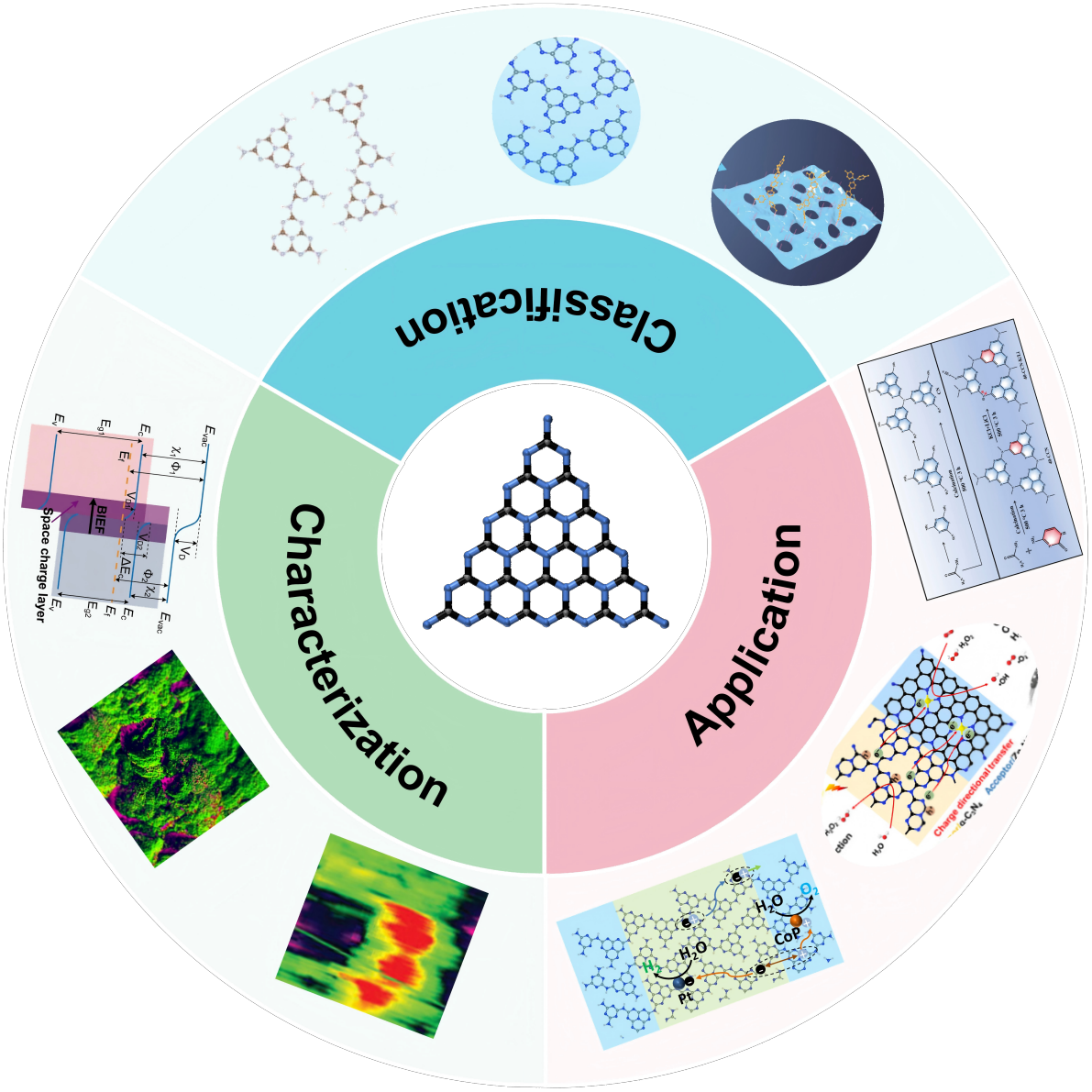

Figure 1. The overview of g-C_3N_4-based molecular junctions. *© 2023 Wiley-VCH GmbH. Copyright © 2021, American Chemical Society. Copyright © 2025, American Chemical Society. © 2025 Wiley-VCH GmbH. Copyright © 2024, American Chemical Society.*

is imperative to catalyze further exploration of their potential in both fundamental scientific research and practical applications.

2 Overview of Carbon Nitride Molecular Junction Materials

2.1 Electronic Structure of g-C_3N_4

Pristine g-C_3N_4 exhibits intrinsic n-type semiconducting characteristics, an attribute primarily ascribed to the prevalence of terminal amino moieties (-NH/NH_2) that function as prototypical electron donors [25]. The foundational architecture is comprised of tri-s-triazine subunits interconnected via secondary nitrogen atoms, wherein the hybridization states of the constituent carbon and nitrogen atoms dictate the global electronic framework. Specifically, the highest occupied molecular orbital (HOMO) of g-C_3N_4 is predominantly composed of N 2p and N 2s hybrid orbitals, with auxiliary contributions from C 2p and C 2s orbitals. The sp^3 hybridization of C and N atoms engenders high-energy σ and σ^* orbitals, while their sp^2 hybridization manifests as lower-energy π molecular orbitals and π^* antibonding orbitals; notably, this π-conjugated framework is identified as the fundamental origin of the photocatalytic activity in g-C_3N_4 [26].

The lone pairs of the sp^2-hybridized N atoms occupy energy levels superior to the π orbitals, thereby

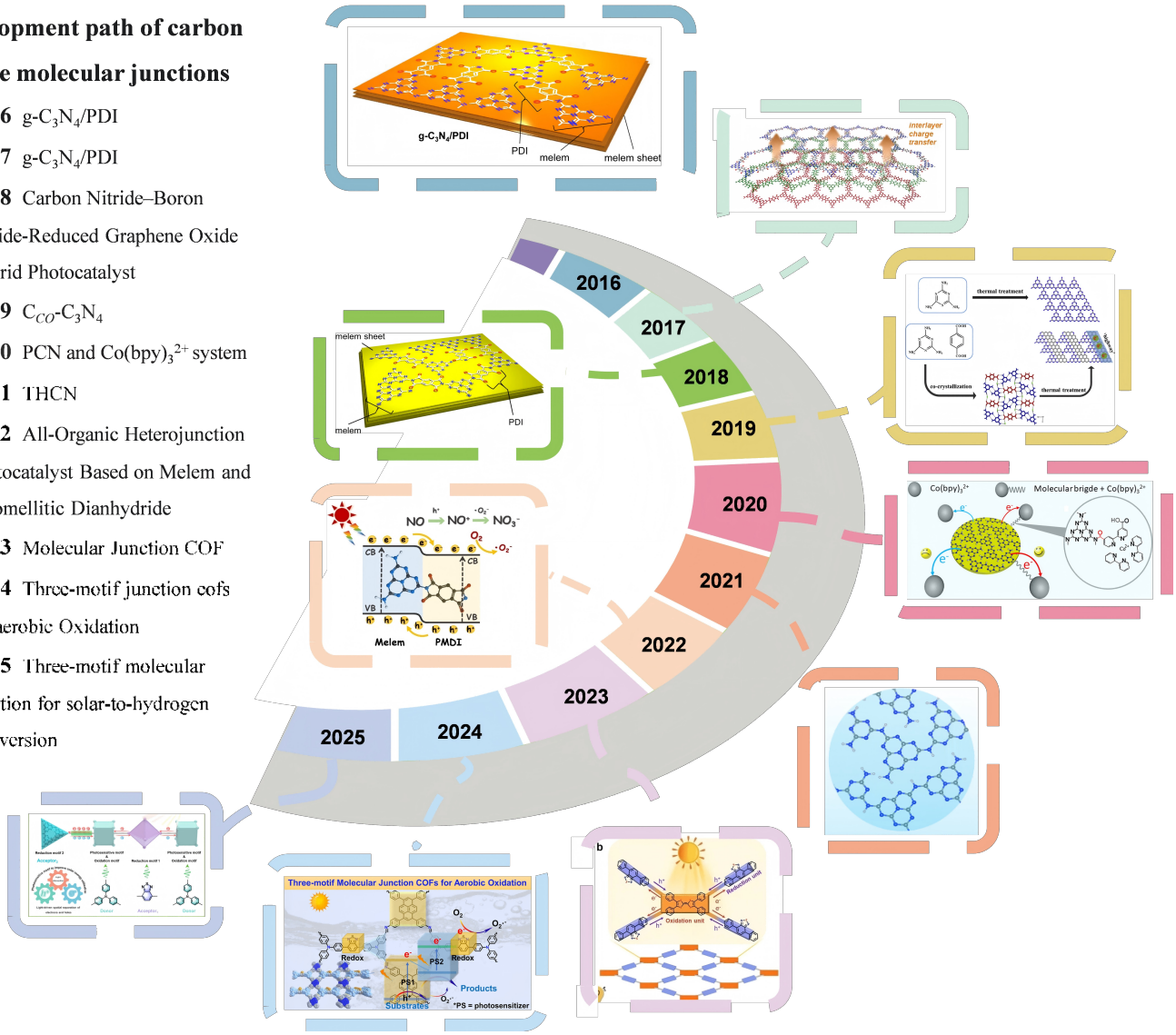

Figure 2. Timeline of progress in g-C_3N_4-based molecular junctions. *Copyright © 2016, American Chemical Society* [15]. *Copyright © 2017, American Chemical Society* [16]. *© 2018 Wiley-VCH Verlag GmbH & Co. KGaA, Weinheim* [17]. *© 2019 The Authors* [18]. *© 2020 Wiley-VCH Verlag GmbH & Co. KGaA, Weinheim* [19]. *Copyright © 2021, American Chemical Society* [20]. *© 2022 Wiley-VCH GmbH* [21]. *© 2022 Wiley-VCH GmbH* [22]. *Copyright © 2024, American Chemical Society* [23]. *Copyright © 2025, American Chemical Society* [24].

establishing n-states situated above the π valence band (Figure 3(A)) [27]. Consequently, two distinct electronic transition pathways exist within g-C_3N_4: the $\pi \rightarrow \pi^*$ transition and the n$\rightarrow \pi^*$ transition. Upon photoexcitation, electrons undergo $\pi \rightarrow \pi^*$ transitions, resulting in an absorption edge at approximately 460 nm in the visible region, which corresponds to a bandgap of 2.7 eV. Simultaneously, the n$\rightarrow \pi^*$ transition facilitates an electronic leap from the n-states to the π^* orbitals, typically manifested as a redshift in the absorption edge or the emergence of a localized absorption tail. However, owing to the spatial orthogonality between the lone pair n-states of the N atoms and the planar conjugated framework, the n$\rightarrow \pi^*$ transition is symmetry-forbidden in a perfectly symmetric tri-s-triazine configuration.

Enhancing the $n \rightarrow \pi^*$ transition efficacy is a critical avenue for augmenting light harvesting and liberating a higher density of photoexcited electrons. This can be achieved through the integration of exogenous photoactive species or heteroatoms to reposition the lone pair states, thereby inducing structural distortions or creating novel intermediate states within the bandgap that facilitate electronic transitions to the π^* orbitals. Furthermore, g-C_3N_4 inherently lacks both vacant and occupied s/p-band centers necessary for the chemisorption of reactive intermediates. The strategic introduction

of foreign atoms to modulate these band centers can provide unpaired electrons or specific orbitals for the optimized adsorption and activation of intermediates. Consequently, tailoring the electronic architecture of g-C_3N_4 serves as a multi-dimensional strategy to bolster light-harvesting capacity, suppress charge-carrier recombination, optimize spatial charge distribution, and accelerate surface reaction kinetics.

2.2 Principles

In this context, the concept of a "molecular junction" can be more precisely defined as an atomically integrated electronic structure in which distinct functional units are covalently bonded within a continuous framework, enabling direct molecular orbital hybridization and extended π-conjugation across the junction. Unlike conventional heterojunctions formed by physical contact between discrete phases, molecular junctions are intrinsically intramolecular in nature, where the interface is not a geometric boundary but a chemically bonded electronic continuum. This fundamental distinction leads to markedly different charge-transfer mechanisms. In traditional heterojunctions, charge separation relies on band alignment and carrier diffusion across a physically defined interface, often accompanied by interfacial resistance, lattice mismatch, and trap states [29, 30]. In contrast, molecular junctions operate through intramolecular charge redistribution driven by differences in local electronic structure, which induces BIEF across the conjugated system. Charge carriers can migrate along delocalized π-orbital pathways with minimal scattering and without crossing discrete phase boundaries [31]. This "in-plane" and "bond-mediated" transport mechanism significantly reduces charge transfer resistance and enables ultrafast and directional carrier separation.

As illustrated in Figure 3(B), the fundamental mechanism governing the photocatalytic process primarily encompasses a sequence of four pivotal stages, beginning with photoexcitation and charge generation. Upon absorbing photon energy ($hv \geq E_g$), the photocatalyst produces photo-induced excitons that subsequently dissociate into free electrons and holes; however, a significant fraction of these carriers undergoes rapid recombination driven by internal Coulombic forces. The surviving charge carriers then engage in directional migration, facilitated by electrostatic forces and internal electric fields. During this transport process, while certain carriers are localized by deep or shallow trapping states, the remainder successfully reach and accumulate at the designated reactive sites.

The efficacy of the subsequent surface redox reactions is highly dependent on the modulation of the electronic structure and surface states, which collectively regulate the thermodynamic redox potentials and kinetic energy barriers for various reaction pathways. Consequently, the concentrated electrons and holes at these active sites drive the corresponding interfacial redox transformations. The catalytic cycle is ultimately concluded by the desorption of final products from the active sites, thereby restoring the photocatalyst to its initial state for subsequent cycles. Taken together, this mechanistic framework underscores that the overall photocatalytic efficiency can be systematically enhanced through the strategic and purposeful optimization of these constituent electronic and chemical procedures.

In bulk g-C_3N_4, the migration of photogenerated electrons is severely hindered by the high energetic barriers associated with interlayer hopping, which significantly limits overall charge carrier mobility. Consequently, the construction of molecular junctions has emerged as a preeminent strategy to circumvent this bottleneck [32]. Distinct from conventional heterojunctions characterized by physical contact, molecular junctions leverage the abundant amine groups and dangling bonds at the g-C_3N_4 edges to facilitate robust covalent anchoring with graphene derivatives, organic conjugated molecules, or triazine/heptazine motifs via chemical pathways such as amidization [33–36], Schiff-base reactions [37], or dehydration condensation. This sophisticated covalent molecular engineering offers unprecedented advantages in modulating charge dynamics that surpass those of traditional physical heterostructures [38, 39]. At the electronic structure level, the grafting of exogenous components induces profound hybridization of molecular orbitals through covalent linkages, substantially extending the delocalization of the π-conjugated system. Such orbital overlap not only redistributes local charge density but also effectively mitigates the localization of charge carriers—a feat difficult to achieve in systems relying solely on interfacial physical contact. From the perspective of band engineering, the disparities in band structures and work functions between constituents drive a realignment of Fermi levels, establishing a potent BIEF within the conjugated plane. The vector of this BIEF, oriented parallel to the basal plane, directs the spatial migration of carriers

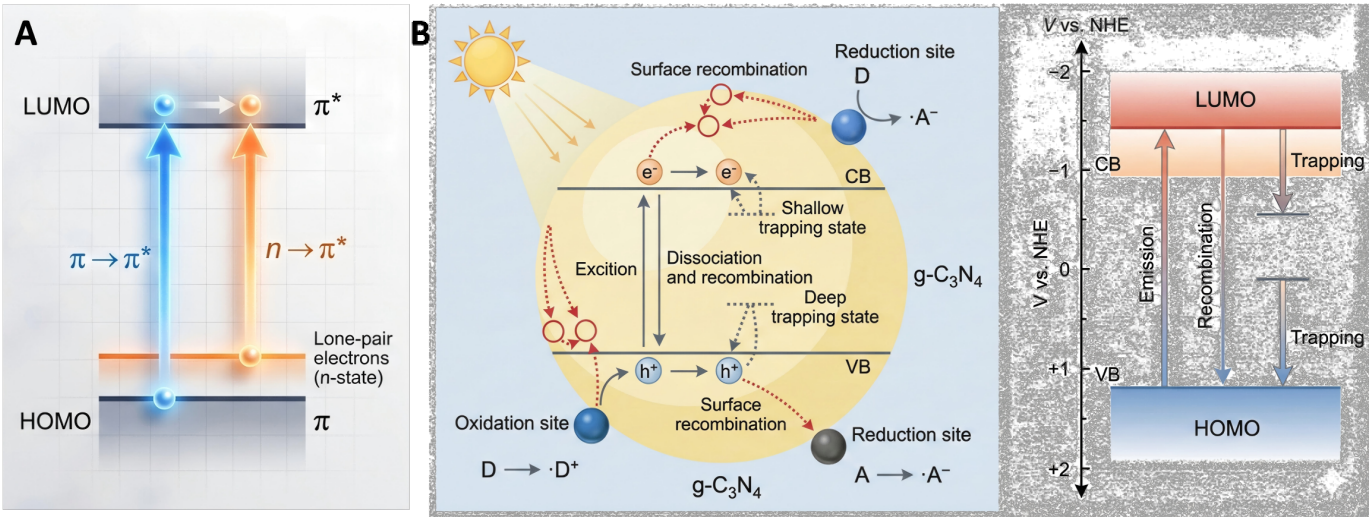

Figure 3. Schematic illustration of electronic structure and photocatalytic process: (A) molecular orbital of g-C_3N_4. (B) photocatalytic process for various applications [28].

along pathways such as Type-I, Type-II, S-scheme, or Schottky barriers. Crucially, these in-plane junctions fundamentally transform the charge transport landscape. In conventional heterostructures, electron transfer is restricted by weak interlayer coupling, necessitating the traversal of formidable vertical barriers across limited interfacial contact areas. In stark contrast, molecular junctions, owing to their structural compatibility and covalent bridging, provide a "high-speed channel" characterized by low resistance for the lateral transport of free electrons and holes within the 2D plane. To quantitatively evaluate the charge transport resistance, the electrochemical impedance spectroscopy (EIS) is widely employed. In a typical Nyquist plot, the semicircle observed in the high-to-medium frequency region corresponds to the interfacial charge transfer process. By fitting the impedance spectra using an equivalent circuit model, the charge transfer resistance (R_{ct}) value can be extracted as the diameter of the semicircle. A smaller R_{ct} indicates a lower interfacial energy barrier and faster charge transfer kinetics. In molecular junction systems, the introduction of BIEF effectively reduces R_{ct} by creating a directional electrostatic driving force that facilitates charge migration across the interface. Meanwhile, the extended π-conjugation and strong electronic coupling provided by covalent linkage further decrease carrier scattering and hopping barriers [40, 41]. This architecture minimizes migration distances and bypasses the high recombination risks inherent in interlayer hopping, thereby achieving highly efficient, anisotropic charge separation. The quintessence of molecular junction design lies in the molecular-level engineering of continuous conjugated interfaces to govern in-plane electronic behavior, rather than mere reliance on band alignment.

2.3 Classification

The core of in-plane junction construction lies in leveraging covalent bonding to achieve atomic-level integration between the g-C_3N_4 framework and functional units, thereby enabling precise modulation of the electronic structure at the molecular level. Based on the disparities in component constitution and electronic energy levels, the synthesis of molecular junctions typically follows two distinct pathways: first, the construction of homojunction interfaces with energy level offsets through the ordered arrangement of g-C_3N_4 homo-isomeric units or the fine-tuning of crystallinity; and second, the realization of covalent coupling between disparate chemical moieties via the introduction of exogenous organic conjugated molecules or graphene derivatives. This classification, grounded in compositional characteristics, not only reflects the diversity of interfacial chemical bonding modes but also fundamentally dictates the magnitude of BIEF and the topological logic of charge carrier migration pathways. This section will elaborate on the construction strategies of these two categories of molecular junctions and their underlying mechanisms in photocatalysis.

2.3.1 Homojunctions

Homojunction frequently referred to as isotype junctions or phase junctions—denote the in-situ construction of in-plane interfaces with well-defined energy level gradients within a singular g-C_3N_4 matrix

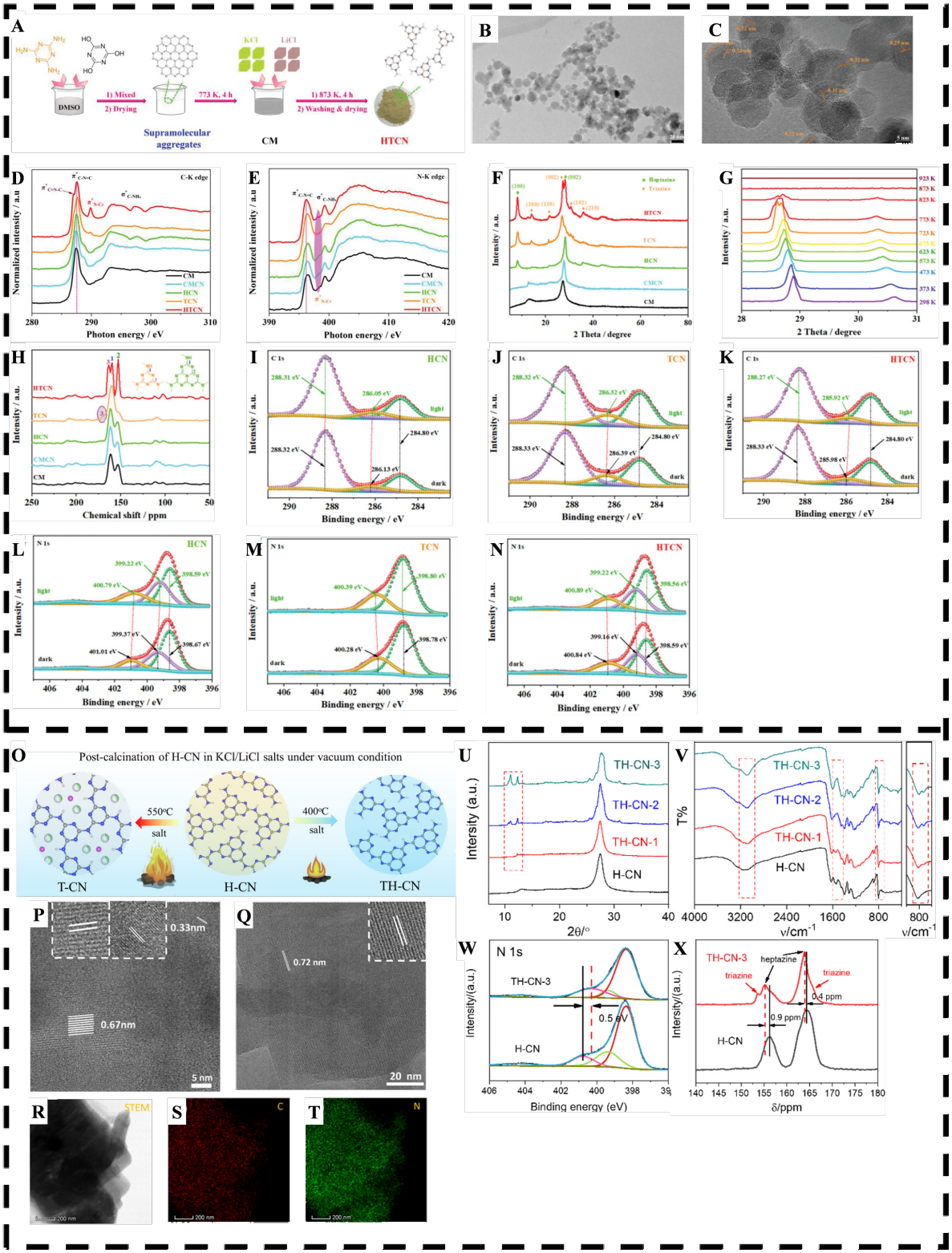

Figure 4. (A) Representation of the synthetic process of HTCN. (B, C) HR-TEM images of HTCN. (D) C K-edge and (E) N K-edge NEXAFS spectra of CM, CMCN, HCN, TCN, and HTCN. (F) XRD and (G) ^{13}C NMR of CM, CMCN, HCN, TCN, and HTCN. (H) In situ XRD spectra of CM and KCl/LiCl composites under different temperatures from 303 to 923 K. XPS spectra of (I-K) C 1s and (L-N) N 1s of HCN, TCN, and HTCN, respectively. © 2023 Wiley-VCH GmbH. (O) Diagram of Synthesis of T–CN and TH–CN by Post-calcination of H–CN in KCl/LiCl Salts under Vacuum Condition. (P)TEM and (Q) HRTEM images of TH–CN-3 sample. (R) STEM image and EDX elemental mapping of (S) C and (T) N for the TH–CN-3 sample. (U) Powder XRD, (V) FTIR, (W) XPS, and (X) solid state ^{13}C NMR spectra of H–CN and TH–CN-x samples. *Copyright © 2021, American Chemical Society.*

by exploiting its inherent structural diversity and polymorphism. This is achieved through the precise manipulation of the polymerization degree, crystalline phases, or local topological subunits. Despite a predominantly uniform chemical composition of carbon and nitrogen, fundamental disparities exist between different structural units or distinct crystalline phases regarding their electronic structures, bandgap widths, and frontier orbital potentials. This "homo isomeric" characteristic drives the realignment of Fermi levels at the interface, thereby spontaneously inducing the formation of BIEF.

The paramount advantage of constructing such homojunctions resides in their capacity to guarantee perfect lattice matching and a continuous π-conjugated system, thereby minimizing the lattice mismatches and interfacial defect centers that frequently plague traditional heterostructures. Consequently, this architectural design facilitates the seamless transport of photogenerated charge carriers through low-impedance channels. The heptazine-triazine (H/T) molecular junction stands as a quintessential paradigm of this strategic approach [42–46].

Zhang et al. [47] developed a molten-salt-assisted synthetic strategy (Figure 4(A)), successfully constructing periodic heptazine–triazine (H/T) molecular junctions within a crystalline carbon nitride framework. High-resolution transmission electron microscopy (HR-TEM) images clearly reveal the morphological characteristics of the resulting HTCN material (Figure 4(B, C)). The successful incorporation of triazine units and their precise chemical environments were systematically confirmed through C and N K-edge near-edge X-ray absorption fine structure (NEXAFS) spectroscopy (Figure 4(D, E)), combined with powder X-ray diffraction (XRD) analysis (Figure 4(F)) and solid-state ^{13}C nuclear magnetic resonance (NMR) spectroscopy (Figure 4(G)). Furthermore, in situ XRD patterns elucidated the structural evolution of the CM and KCl /LiCl composite during the controlled heating process (Figure 4(H)). High-resolution X-ray photoelectron spectroscopy (HRXPS) analysis revealed binding energy shifts in the C 1s (Figure 4(I-K)) and N 1s (Figure 4(L-N)) orbitals across HCN, TCN, and HTCN, validating the modulation of the electronic structure. This structural refinement facilitates the formation of long-lived shallow trap states which, in synergy with BIEF, effectively extend charge carrier lifetimes. This mechanism drives the directional migration of electrons toward the triazine units, thereby enhancing the efficiency of photocatalytic H_2O_2 production.

Expanding upon the paradigm of molecular junction engineering, Pan and co-workers elucidated the critical function of H/T junctions in mediating visible-light-driven overall water splitting [20]. Through a vacuum-assisted molten-salt post-treatment of H-CN, the precise structural evolution into T-CN and TH-CN architectures was systematically controlled (Figure 4(O)). The formation of an intimate, atomic-level heterointerface within the TH-CN matrix was unambiguously corroborated by TEM/HRTEM (Figure 4(P, Q)) alongside scanning transmission electron microscopy-energy-dispersive X-ray spectroscopy (STEM-EDX) elemental mapping (Figure 4(R-T)). Comprehensive structural and electronic elucidations—encompassing powder XRD (Figure 4(U)), Fourier-transform infrared (FTIR) spectroscopy (Figure 4(V)), XPS (Figure 4(W)), and solid-state ^{13}C NMR (Figure 4(X))—collectively demonstrated that the integration of this molecular junction profoundly attenuates the exciton binding energy. The resultant interfacial energy offset provides a robust thermodynamic driving force for spontaneous exciton dissociation. Consequently, this engineered energetic landscape endows the modified polymeric framework with exceptional photocatalytic efficacy, culminating in the stoichiometric evolution of H_2 and O_2.

2.3.2 *Molecular Heterojunctions*

Unlike homojunctions that rely solely on structural heterogeneity within the framework, heterojunctions provide a more versatile strategy for tailoring the electronic structure of photocatalysts [48, 49]. The core design philosophy lies in the covalent integration of the g-C_3N_4 framework with chemically distinct external organic components, metal active centers, or multifunctional molecular units at the atomic level, thereby constructing strong donor–acceptor (D–A) coupling across molecular interfaces [50, 51].

From a physical perspective, the advantages of such hetero-structural design originate from its ability to reconfigure charge-carrier dynamics in multiple dimensions [52]. First, the introduction of hetero units with markedly different work functions can generate strong in-plane molecular dipole moments, establishing a much steeper electrostatic potential gradient and consequently a stronger BIEF than those in homogeneous systems. Second, the incorporation of hetero components often modifies the density of

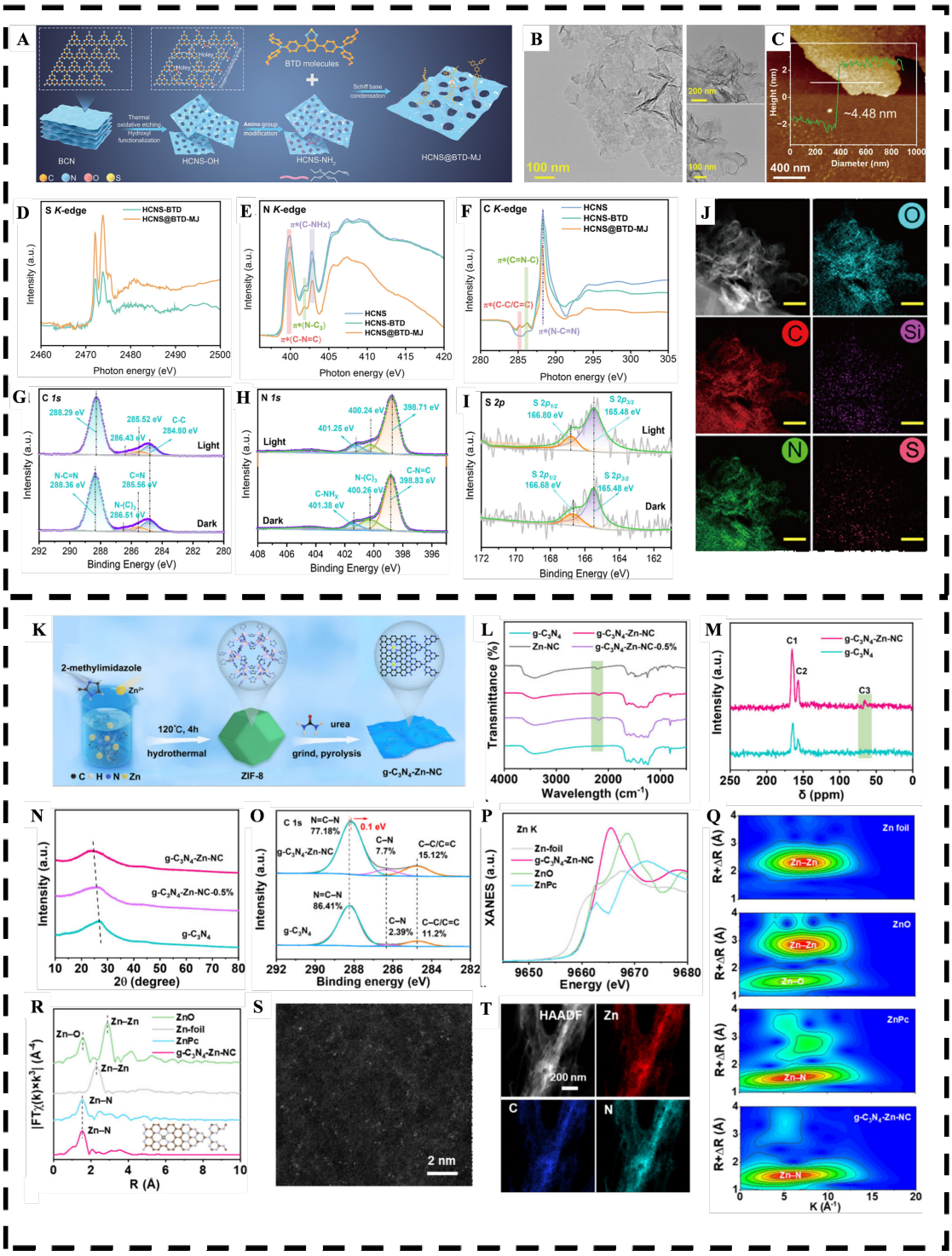

Figure 5. (A)Schematic illustration of the synthesis route of HCNS@BTD-MJ. (B) TEM images. (C) AFM images and the corresponding height profiles. XANES spectra of the (D) C K-edge and (E) N K-edge of HCNS, HCNS–BTD, and HCNS@BTD-MJ. (F) S K-edge XANES spectra of H CNS–BTD and HCNS@BTD-MJ. (G-I) ISI-XPS spectra of C 1s, N 1s, and S 2p for HCNS@BTD-MJ samples before and after light illumination. (J) HAADF-STEM image of HCNS@BTD-MJ and the corresponding EDX elemental mapping images of C, N, O, Si, and S. *Copyright © 2025, American Chemical Society*. (K) Schematic illustration of g-C_3N_4-Zn-NC. (L) FTIR spectra of thus-prepared samples. (M) Solid-state ^{13}C NMR spectra of g-C_3N_4 and g-C_3N_4-Zn-NC. (N) XRD patterns of g-C_3N_4, g-C_3N_4-Zn-NC-0.5%, and g-C_3N_4-Zn-NC. (O) High-resolution C 1s XPS spectra of g-C_3N_4 and g-C_3N_4-Zn-NC. (P) Zn K-edge XANES, (Q) WT for the EXAFS signals of g-C_3N_4-Zn-NC, ZnO, ZnPc, and Zn foil and(R) EXAFS spectra (the inset shows the structural model). (S) AC-HAADF-STEM and (T) HAADF-STEM images with the corresponding EDS mapping images of g-C_3N_4-Zn-NC. *Copyright © 2024, American Chemical Society*.

electronic states, and may even induce the formation of an intermediate band, which not only broadens the light absorption range but also provides additional electronic transition pathways that facilitate charge separation. Finally, the precise spatial arrangement of hetero units enables the physical separation of oxidation and reduction sites, thereby fundamentally suppressing the spatial recombination of charge carriers. Current advances in this field are mainly centered on several representative design strategies.

Conventional heterojunctions are typically based on binary systems, whereas recent studies are increasingly moving toward more complex molecular architectures featuring multiple building motifs and charge-transfer channels. For example, Xiao and co-workers reported a three-motif molecular junction with significant conceptual importance (Figure 5(A)). In this work, a D–A–D type photosensitive molecule was covalently bridged onto the surface of porous carbon nitride nanosheets (HCNS), forming the HCNS@BTD-MJ composite system [52]. TEM (Figure 5(B)) and Atomic Force Microscope (AFM) images (Figure 5(C)) clearly reveal its distinctive morphology and nanoscale thickness distribution. Meanwhile, X-ray absorption near-edge structure (XANES) analyses at the C and N K-edges (Figure 5(D,E)), together with the S K-edge spectra (Figure 5(F)), confirm the successful chemical modification between HCNS and the BTD unit as well as the well-defined molecular coordination environment [53].

This structural design establishes spatially separated dual reduction sites, where the molecular-level energy gradient efficiently drives photogenerated electrons from the photosensitive unit toward the reduction centers. To directly probe the charge-transfer process, in situ irradiation X-ray photoelectron spectroscopy (ISI-XPS) was employed. The binding-energy shifts of the C 1s, N 1s, and S 2p orbitals before and after illumination (Figure 5(G–I)) provide direct evidence for the directional migration of photogenerated electrons. In addition, High-Angle Annular Dark-Field Scanning Transmission Electron Microscopy (HAADF-STEM) imaging combined with EDX elemental mapping (Figure 5(J)) further verifies the homogeneous distribution of C, N, O, Si, and S elements throughout the three-motif junction. As a result, this multi-motif integration significantly promotes the dissociation of excitons into free charge carriers, enabling outstanding solar-driven hydrogen evolution performance even without the assistance of expensive cocatalysts.

In parallel, the coupling between catalytic active centers and internal physical fields has recently emerged as a promising paradigm in photocatalysis. Rao and co-workers developed a D–A catalytic system regulated by atomic Zn-N4 sites [54]. In this heteromolecular junction, g-C_3N_4 functions as the electron donor, while the acceptor component Zn-NC, containing anchored single-atom Zn sites, is seamlessly integrated through $\pi - \pi$ conjugation interactions [55–57]. Notably, the introduction of Zn-NC induces an intermediate band within the bandgap, which significantly enhances visible-light absorption. Meanwhile, the local polarization electric field generated by the Zn center greatly accelerates the injection of photogenerated electrons into the catalytic active sites. The resulting BIEF-driven charge separation leads to the rapid generation of reactive oxygen species (ROS), thereby endowing the heteromolecular junction with remarkably enhanced photocatalytic antibacterial activity.

3 Precise Characterization Techniques for Built-in Electric Fields

The precise construction and modulation of molecular junctions in g-C_3N_4 have emerged as a cutting-edge research frontier in photocatalytic materials. As a prototypical two-dimensional material, g-C_3N_4 exhibits unique advantages in achieving efficient photocatalytic conversion. However, its inherent low crystallinity and highly disordered microstructure impose significant limitations on the direct observation of molecular junction fine structures. Although the advent of advanced characterization techniques has provided preliminary experimental evidence for the existence of in-plane junctions, the qualitative and quantitative analysis of interfacial physicochemical properties at the atomic scale, as well as the establishment of structure-activity relationships with charge carrier transport behavior, remains a critical scientific challenge in this field. BIEF induced by molecular junctions serves as a crucial factor in controlling the separation and transport efficiency of photogenerated charge carriers. Accurate characterization of its intensity distribution is essential for understanding photocatalytic mechanisms. This section systematically reviews recent progress in multiscale characterization techniques, particularly focusing on their applications in atomic-scale structure determination, BIEF dynamic evolution, and spatiotemporal carrier dynamics. These advances provide both theoretical insights and technical support for developing high-performance g-C_3N_4-based

photocatalysts.

In the design of advanced photocatalytic systems, the precise construction of molecular junctions and a thorough understanding of the regulation of BIEF are central to achieving efficient charge separation. Taking asymmetric molecular-junction-modified carbon nitride as an example [35], the identification of BIEF follows a comprehensive evaluation framework that spans static electronic distribution to dynamic excited-state behavior.

The analysis first focuses on charge non-uniformity at the molecular scale. High-resolution XPS reveals binding-energy shifts in the C 1s (Figure 6(B)) and N 1s (Figure 6(C)) spectra, which serve as direct spectroscopic evidence of electronic coupling between heterogeneous units. The underlying physical origins lie in the fact that when the electron density around atoms is altered by chemical bonding, the shielding effect on inner-shell electrons correspondingly changes, resulting in shifts in core energy levels. Such spectral variations provide direct evidence for interfacial charge redistribution caused by electronegativity differences between molecular components. At the theoretical level, DFT calculations further elucidate the electronic structure evolution. The calculated density of states (Figure 6(F–H)) reveals the localized modification of the band structure induced by the introduction of heteroatoms. Meanwhile, the spatial distributions of HOMO and LUMO (Figure 6(I–K)) quantitatively illustrate, from a quantum-chemical perspective, the molecular dipole moments generated by symmetry breaking within the structure. Together, these results provide a theoretical basis for defining both the physical origin and driving strength of the BIEF.

To visualize the spatial distribution of the internal physical field, KPFM plays a crucial role. KPFM maps the surface work-function distribution by measuring the contact potential difference (CPD) between the probe and the sample surface. By comparing the surface potential images of CN, CN-G, and CN-X (Figure 6(M–O)), the existence of BIEF is not only confirmed but the potential step at the molecular interface is also clearly mapped. In addition, zeta-potential measurements (Figure 6(L)) further corroborate the variation in surface polarity from the perspective of interfacial charge characteristics. As shown in Figure 6(L), all photo-catalysts (CN, CN-G, and CN-X) exhibit negative surface charges, with the absolute values progressively increasing. This indicates stronger electrostatic forces and higher charge energy [58, 59].

For example, Li and co-workers successfully constructed in-plane molecular junctions by introducing purine molecules with highly asymmetric electronic structures into the g-C_3N_4 framework [35]. Their results clearly demonstrate that the BIEF acts as the key driving force directing photogenerated electrons toward catalytic active sites. In another representative study, Zhang and co-workers fabricated a heptazine-triazine (H/T) molecular junction (Figure 4(A)) [47]. Using in situ photo-irradiated KPFM, they observed a dynamic shift in CPD under light excitation (Figure 6(T)), indicating that both the strength and directionality of the internal electric field continuously increase upon the formation of the H/T molecular linkage.

Notably, the HTCN sample exhibits the largest light-induced CPD shift, with BIEF intensity 4.2 times higher than that of CM (Figure 6(T)). These observations suggest that the H/T molecular junction can rapidly drive electron migration along the potential gradient immediately upon photoexcitation, enabling the in situ visualization of charge-drift direction [60]. By capturing the work-function evolution associated with the migration of photogenerated carriers toward the surface under BIEF driving, this technique directly maps the vectorial direction of charge transport, effectively transforming the otherwise abstract internal electric field into a spatially resolved potential landscape.

The regulatory effect of BIEF on charge carriers ultimately extends to the microscopic dynamics of excited states. Femtosecond transient absorption spectroscopy (fs-TAS) (Figure 6(V–Z)), a key technique for probing ultrafast processes [61, 62], provides detailed insight into the generation, evolution, and decay of excited-state species. In the spectra, the negative signal in the 440–580 nm region originates from ground-state bleaching, whereas the positive band at longer wavelengths corresponds to the excited-state absorption (ESA) of shallow-trapped electrons. Notably, HTCN exhibits the strongest and longest-lived ESA signal, indicating that the H/T molecular junction significantly increases both the population and stability of shallow-trapped electrons.

From a mechanistic perspective, the enhancement of the ESA signal in HTCN can be directly correlated with the role of the BIEF in modulating exciton dynamics on the femtosecond timescale. The BIEF

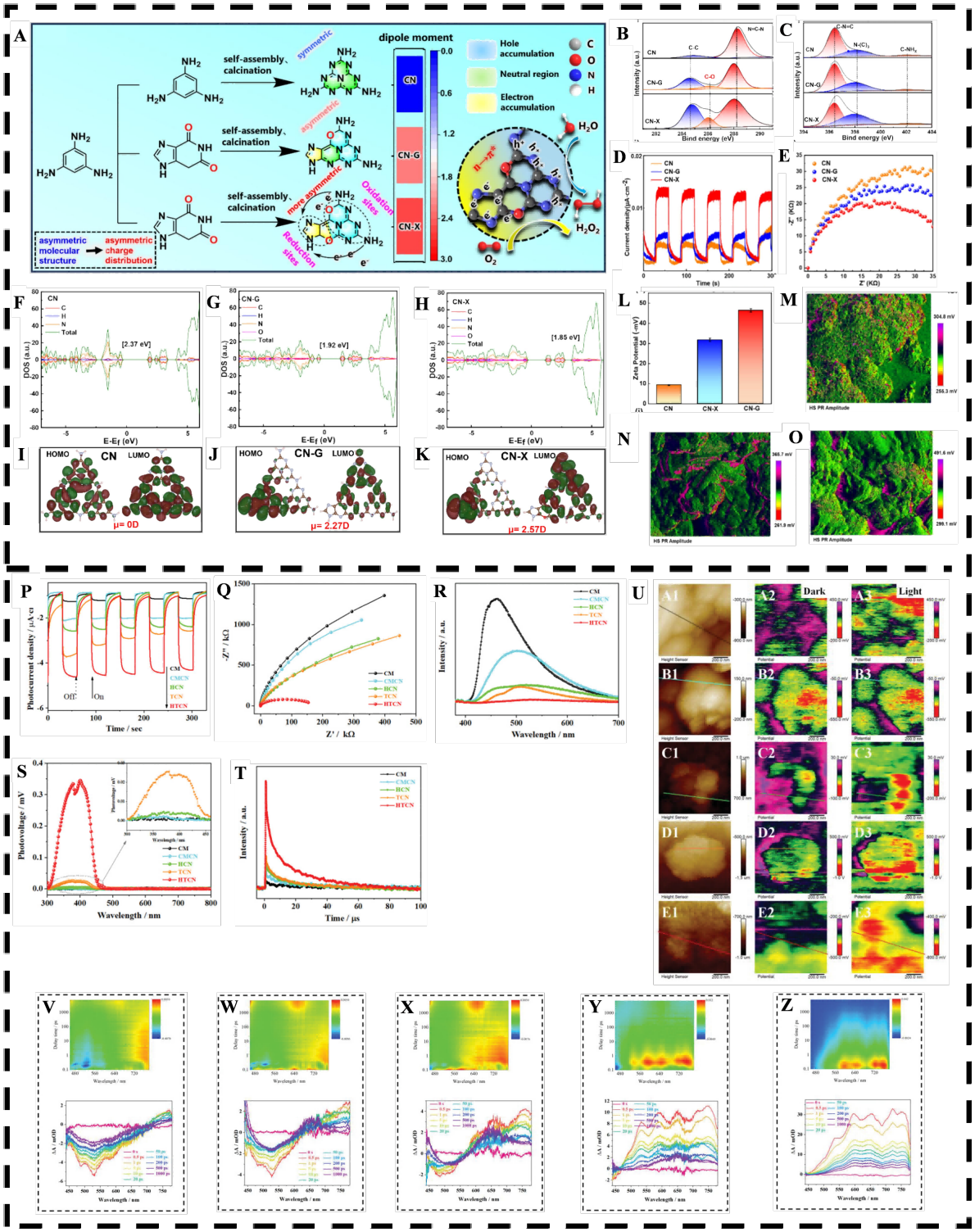

Figure 6. (a) Scheme of the synthetic procedure for the CN-G and CN-X. XPS spectra of (B) C 1s, (C) N 1s. (D) transient photocurrent response curves, (E) electrochemical impedance spectra Calculated DOSs for (F) CN, (G) CN-G, (H) CN-X. (I-K) HOMO-LUMO plots and molecular dipole moments. (L) Zeta potentials. KPFM images of (M) CN, (N) CN-G, (O) CN-X. P) Transient photocurrent response, and Q) EIS spectra of CM, CMCN, HCN, TCN, and HTCN. R) PL spectra, S) SPV spectra, T) TPV spectra. U) Surface morphologies (A1, B1, C1, D1, E1) and corresponding surface potential images in the absence (A2, B2, C2, D2, E2) and presence (A3, B3, C3, D3, E3) of light for (A) CM, (B) CMCN, C) HCN, D) TCN, and E) HTCN, respectively. 3D contour plots of fs-TAS recorded at indicated delay times measured with 400 nm excitation: (V) CM, (W) CMCN, (X) HCN, (Y) TCN, and (Z) HTCN.

generated by the heptazine-triazine molecular junction introduces an internal electrostatic potential gradient that effectively screens the Coulombic attraction between photogenerated electrons and holes. This field-induced screening reduces the exciton binding energy and lowers the energetic barrier for exciton dissociation. More importantly, the presence of a directional electric field provides an additional driving force that accelerates the spatial separation of electron–hole pairs immediately after photoexcitation. As a consequence, excitons can be dissociated into free carriers within an ultrafast timescale, leading to a higher population of free or shallow-trapped electrons. This increased carrier population is directly reflected in the intensified ESA signal observed in fs-TAS spectra. The enhanced ESA signal in HTCN is not only indicative of improved carrier lifetime, but also serves as strong evidence for BIEF-assisted ultrafast exciton dissociation.

The strong internal electric bias generated by the H/T molecular junction effectively overcomes Coulombic attraction, reduces the exciton binding energy, and promotes the rapid conversion of excitons into free charge carriers [63]. Consequently, the prolonged and intensified ESA signal observed in HTCN not only reflects the presence of an internal electric field but also demonstrates that this field breaks exciton confinement on the femtosecond timescale, allowing excitons to transition into free carrier states at a very early stage after photoexcitation [64, 65].

Such field-driven effects are further verified by surface photovoltage (SPV) (Figure 6(S)) and transient photovoltage (TPV) (Figure 6(T)) measurements, which probe carrier dynamics on slower timescales. In the SPV response, HTCN exhibits the most pronounced photoinduced surface potential, suggesting that on the nanosecond to microsecond timescale, charge carriers can still be continuously driven toward the surface under the influence of BIEF. Meanwhile, the TPV decay curves reveal a significantly prolonged voltage lifetime for HTCN, indicating that charge recombination is effectively suppressed under the protection of the internal electric field. In essence, SPV reflects the directional diffusion capability of charge carriers under BIEF, whereas TPV reveals the interfacial charge recombination kinetics; together, these results confirm the significant enhancement of carrier diffusion length and separation efficiency.

Photoelectrochemical characterizations of HTCN (Figure 6(P-Q)) further show that it delivers the highest transient photocurrent and the lowest interfacial charge-transfer resistance, reinforcing the effectiveness of the H/T molecular junction as a key structural unit for charge separation [66]. By integrating structural characterization, potential imaging, ultrafast spectroscopy, and interfacial charge-transport analysis, a comprehensive evidence chain emerges: the H/T molecular junction strengthens the internal BIEF, which continuously drives directional electron migration and separation across the entire temporal scale—from femtosecond excited-state processes to steady-state surface accumulation. This multiscale charge-regulation mechanism ultimately leads to a systematic enhancement of photocatalytic performance.

This complementary characterization system, encompassing "structural origin-theoretical quantification-in situ imaging-ultrafast kinetic response," ultimately achieves a comprehensive macroscopic electrochemical closure. The leap in photocurrent intensity (Figure 6(R, D)) reflects enhanced steady-state carrier collection efficiency, while the reduced radius of EIS arc (Figure 6(S, E)), attributable to decreased Rct, confirms the significant promotion effect of BIEF on interfacial charge extraction and transport kinetics. Such a multi-dimensional, cross-scale rigorous logical framework not only clearly elucidates the regulation mechanism of asymmetric molecular pairs on electric field intensity but also establishes a solid scientific foundation for designing polar photocatalytic materials with highly efficient charge separation capabilities.

4 Application

4.1 Hydrogen evolution and over water splitting

The direct conversion of solar energy into hydrogen fuel represents one of the most promising strategies for addressing the global energy crisis and achieving carbon neutrality [67, 68]. However, for polymeric semiconductor photocatalysts such as g-C_3N_4, this process faces substantial thermodynamic and kinetic challenges. From a microscopic physical perspective, organic semiconductors typically possess relatively high Frenkel exciton binding energies (E_b), which makes the spontaneous dissociation of photogenerated electron–hole pairs difficult and leads to severe carrier recombination. Moreover, overall water splitting (OWS) involves a complex four-electron transfer process, in which the sluggish surface oxygen evolution reaction (OER) frequently becomes the

rate-determining step (RDS) that limits the overall efficiency [69–71]. Therefore, reducing Eb through band-structure engineering and constructing rapid charge-transport pathways are widely regarded as key strategies for overcoming these intrinsic limitations.

The construction of molecular junctions provides a precise physical-field framework for overcoming exciton confinement and driving complex catalytic reactions. Pan and co-workers fabricated an atomically defined H/T homojunction via an in situ growth strategy (Figure 4(O)) [20]. By modulating the local dielectric environment, the exciton binding energy was significantly reduced, thereby directly overcoming the long-standing limitation that conventional carbon nitride is unable to drive visible-light overall water splitting. Photocatalytic performance measurements (Figure 7(A-C)) show that the TH–CN-2 sample achieves stoichiometric H_2 and O_2 evolution under visible-light irradiation, with a photocatalytic activity 34 times higher than that of pristine H–CN. In addition, wavelength-dependent experiments (Figure 7(D)) reveal that the rates of hydrogen and oxygen evolution closely match the optical absorption profile, further confirming the substantial improvement in photon utilization enabled by the molecular junction.

To address the kinetic challenges associated with photogenerated charge extraction and long-range transport, multicomponent heterojunctions exhibit a remarkable "electron-pump" effect through the construction of multilevel energy gradients. For example, Xiao and co-workers designed a three-motif system, HCNS@BTD-MJ (Figure 5(A)) [24], in which spatially separated dual reduction sites enable highly efficient charge pumping. As shown in the photocatalytic measurements (Figure 7(E-F)), the hydrogen evolution rate of HCNS@BTD-MJ is increased by orders of magnitude compared with pristine BCN and HCNS, and an impressive apparent quantum yield (AQY) of 16.7% at 420 nm is achieved. Moreover, the system demonstrates excellent monochromatic-light adaptability and cycling stability, maintaining nearly unchanged activity over 18 consecutive reaction cycles (Figure 7(I)). A radar chart comparing AQY distributions at different catalyst masses (Figure 7(J)), together with a benchmark comparison with recently reported high-performance photocatalysts (Figure 7(H, K)), further highlights the leading role of the three-motif molecular junction in enhancing solar-to-chemical energy conversion efficiency.

The concept of reinforcing intramolecular dipole moments and constructing D–A energy gradients is also broadly applicable to more complex organic framework systems. Shu and co-workers extended this strategy to sulfone-containing covalent organic frameworks (COFs) (Figure 7(L)) [72]. Through the precise design of D–A–A type molecular units, the resulting FS-OHOMe-COF exhibits significantly enhanced H_2O_2 production activity under visible light, far outperforming that of physically mixed systems (Figure 7(M)). The wavelength-dependent external quantum efficiency (EQE) profile (Figure 7(N)), together with control experiments under different atmospheres (Figure 7(O)), collectively reveals its high efficiency in photogenerated electron utilization.

Taken together, these application examples demonstrate that the molecular-junction strategy not only serves as a general paradigm for constructing efficient solar fuel conversion systems, but also provides a powerful approach for precisely controlling the directional migration of photoinduced charges at the molecular level.

4.2 Selective Conversion of High Value-added Chemicals

The use of photocatalysis for the synthesis of high-value chemicals, such as hydrogen peroxide production and selective oxidation of hydrocarbons, has emerged as an important pathway toward sustainable green chemistry. However, unlike overall water splitting, the central challenge in these reactions lies in achieving high selectivity [73, 74]. Photogenerated holes or ROS usually possess strong oxidative capability, which can easily lead to the overoxidation of target products into the final product CO_2. Similarly, in H_2O_2 production, suppressing the competing four-electron oxygen reduction pathway ($O_2 \rightarrow H_2O$) remains a major challenge. Conventional catalysts often lack the ability to precisely regulate the adsorption configuration of reaction intermediates and the number of transferred electrons, making it difficult to simultaneously achieve high product yield and high selectivity.

The molecular junction strategy provides a precise physical driving force to overcome the "activity-selectivity" trade-off in photocatalysis by tailoring the surface electric field distribution and the electronic structure of active sites at the molecular level. In the field of H_2O_2 photosynthesis, Zhang et al. [47] demonstrated that heptazine-triazine molecular junctions induce the formation of unique,

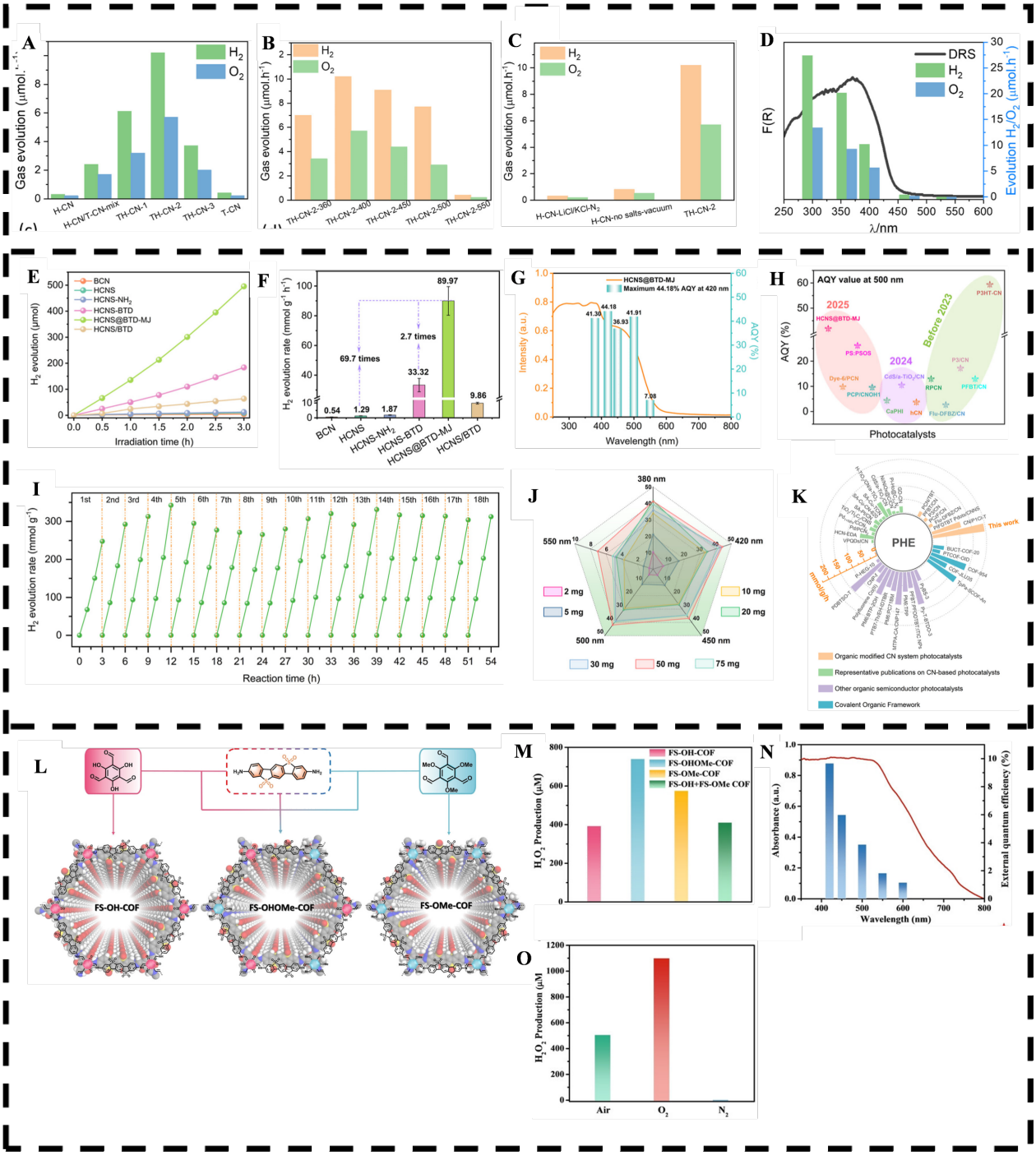

Figure 7. (A) Photocatalytic OWS rate of H–CN, T–CN, H–CN/T–CN-mix and TH–CN-x. (B) Photocatalytic OWS rate of TH–CN-2-x. (C) Photocatalytic OWS rate of H–CN–no salts–vacuum, H–CN–LiCl/KCl–N2 and TH–CN-2. (D) Wavelength dependence OWS activities of TH–CN-2 photocatalyst. *Copyright © 2021, American Chemical Society*. (E) Typical time course of H_2 production for BCN, HCNS, HCNS–NH_2, HCNS–BTD, HCNS@BTD-MJ, and HCNS/BTD. (F) Comparative presentation of the H_2 evolution rates. (G) Optical absorbance-dependent AQY measurement of HCNS@BTD-MJ. (H) Comparison of the AQY at 500 nm of HCNS@BTD-MJ and recently reported photocatalysts. (I) Cyclic stability test of HCNS@BTD-MJ catalysts under continuous operation for 18 cycles. (J) Radar chart of the AQY values for HCNS@BTD-MJ with different catalyst masses. (K) Comparison of the PHE performance with that of different reported photocatalysts. *Copyright © 2025, American Chemical Society*. (L)The synthetic routes and chemical structures of the sulfone COFs(M) Photocatalytic H_2O_2 production performances for FS-OH-COF, FS-OHOMe-COF, FS-OMe-COF and a physical mixture of FS-OH-COF and FS-OMe-COF. (N) EQE of FS-OHOMe-COF at various incident light wavelengths. (O) Photocatalytic reaction under different atmosphere. *© 2024 Wiley-VCH GmbH*.

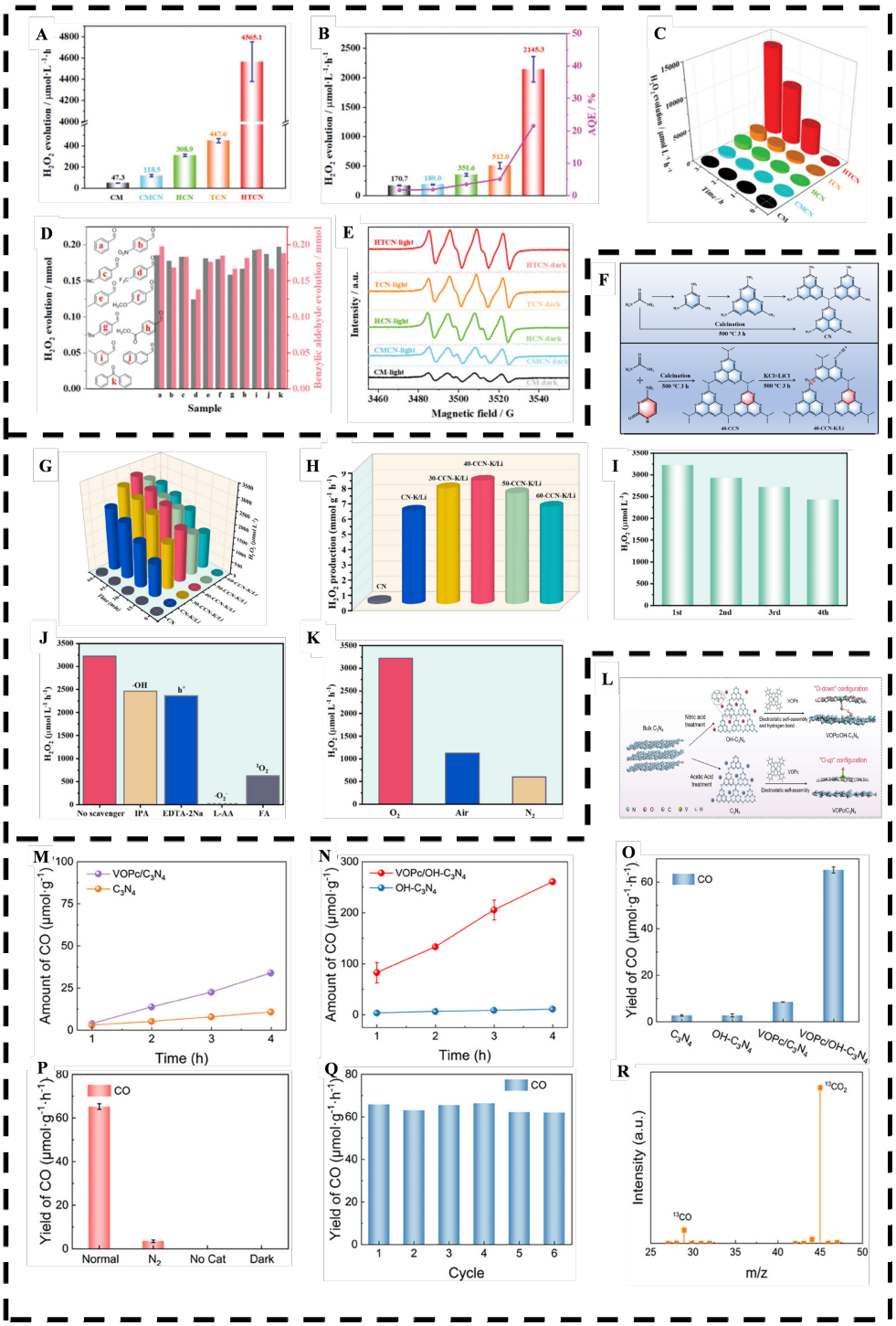

Figure 8. A) Photocatalytic H_2O_2 evolution. B) Photocatalytic H_2O_2 evolution and C) Stability of CM, CMCN, HCN, TCN, and HTCN. D) Photocatalytic H_2O_2 and benzylic aldehyde evolution over HTCN. E) ESR signals of in situ formed DMPO-·O2- for CM, CMCN, HCN, TCN, and HTCN in methanol. *© 2023 Wiley-VCH GmbH* (F) Possible reaction route of CN and 40-CCN-K/Li. (G, H) The performance of photocatalytic H_2O_2 generation by all products. (I) Cycle experiments of photocatalytic H_2O_2 generation by 40-CCN-K/Li. (J) Photocatalytic H_2O_2 generation over 40-CCN-K/Li in the appearance of different radical scavengers. (K) Photocatalytic H_2O_2 generation rate over 40-CCN-K/Li in different atmospheres. *© 2025 Wiley-VCH GmbH.* (L) Schematic representation of the synthesis of VOPc/C3N4 and VOPc/OH-C_3N_4. (M, N) Time-dependence photocatalytic activity and (O) Gas products generation rate over C_3N_4, OH-C_3N_4, VOPc/ C_3N_4, and VOPc/OH-C_3N_4 under simulated solar light irradiation (representing standard deviation, SD). (P) Photocatalytic CO generation on VOPc/OH-C_3N_4 under different conditions. (Q) The CO yields on VOPc/OH-C_3N_4 across six-cycle tests. (R) The mass spectra of ^{13}CO generated under $^{13}CO_2$ atmosphere. *© 2026 Wiley-VCH GmbH.*

long-lived shallow trap states, which significantly enhances both the photocatalytic activity (Figure 8(A, B)) and operational stability (Figure 8(C)). In-situ ESR spectroscopy capturing the DMPO·O_2^- signals (Figure 8(E)) verified that these trap states alter the adsorption mode of oxygen molecules, driving them to adopt a "side-on" configuration that thermodynamically locks in the two-electron oxygen reduction ($2e^-$ ORR) pathway. This strategy not only enabled the efficient accumulation of H_2O_2 but also successfully established a "dual-functional" synthesis system that couples H_2O_2 production with the selective oxidation of benzyl alcohol to benzaldehyde (Figure 8(D)).

To achieve precise control over the reaction kinetics, Zhao et al. [75] engineered a 40-CCN-K/Li system that functions as a "molecular regulatory valve" by tuning the ratio of peripheral donor-acceptor units (Figure 8(F)). Experimental results revealed that this system achieves a linear and precise regulation of the H_2O_2 yield (Figure 8(G, H)) while exhibiting excellent cycling stability (Figure 8(I)). Through radical scavenging experiments (Figure 8(J)) and control experiments under various atmospheres (Figure 8(K)), the study further elucidated the intramolecular charge transport logic, providing a kinetic safeguard to maintain high selectivity in complex reaction environments.

Furthermore, the molecular junction strategy exhibits remarkable regulatory potential in the challenging domain of CO_2 reduction [76]. Xie et al. [77] successfully fabricated a VOPc/OH-C_3N_4 heterointerface with a "molecular switch" effect by dynamically manipulating the orientation of vanadyl phthalocyanine (VOPc) on the surface of hydroxylated carbon nitride (Figure 8(L)). Compared to pristine C_3N_4 or its individual components, the modified system delivered a substantial leap in photocatalytic activity (Figure 8(M, N)). Gas product evolution rate measurements (Figure 8(O)) and high-yield CO evolution data (Figure 8(P)) indicated that the optimization of the interfacial dipole moment drastically facilitates CO_2 activation. Following six testing cycles, the catalyst retained a high degree of activity and stability (Figure 8(Q)). Most compellingly, ^{13}C isotope labeling experiments (Figure 8(R)) unambiguously confirmed that the generated CO originates entirely from the CO_2 reduction process, rather than from the decomposition of the catalyst itself. This series of investigations signifies that photocatalytic synthesis is transitioning from conventional empirical exploration toward a phase of precise control predicated on molecular junction design.

4.3 Deep Regulation of Reactive Oxygen Species and Excitons

In the fields of environmental remediation and biomedicine, the primary mission of photocatalysts is to generate high concentrations of reactive oxygen species such as ·O_2^- and ·OH to tackle complex environmental challenges, including antibiotic residues and pathogenic infections [78–81]. This demands that the catalyst possesses not only appropriate band edge alignments but also ultrafast interfacial charge injection kinetics to prevent charge carrier recombination prior to ROS generation. Conversely, optoelectronic devices (e.g., LEDs) exploit the antithetical physical process—radiative recombination—which imposes stringent requirements on the exciton energy level structure and the photoluminescence quantum yield.

The robust BIEF generated by molecular junctions has emerged as a kinetic engine driving the explosive generation of ROS. Rao et al. [54] successfully constructed heteromolecular junctions with high charge-separation efficiency by precisely engineering atomic-scale Zn-N_4 sites within the g-C_3N_4 framework (Figure 5(K)). In this system, the introduction of Zn single atoms induces an "intermediate band" within the bandgap, which not only effectively broadens the spectral response but also leverages the strong localized electric field to drive the ultrafast injection of photogenerated electrons into the Zn active centers.

In situ ESR spectroscopy (Figure 9(D-G)) confirmed that the system exhibits significantly enhanced generation capabilities for superoxide radicals (O_2^-) and hydroxyl radicals (OH) under both air and argon atmospheres. This efficient radical burst, synergized with high H_2O_2 accumulation (Figure 9(H)), enables the material to demonstrate potent killing efficiency against Methicillin-resistant Staphylococcus aureus (MRSA), S. aureus, and E. coli (Figure 9(A-C)). With increasing irradiation time, the survival rate of pathogenic bacteria decreases logarithmically, fully demonstrating the immense potential of BIEF-induced oxidative stress in the field of bio-antibacterial applications.

Regarding the expansion of optoelectronic functionalities, the molecular junction strategy showcases a capacity for the fine-tuning of exciton

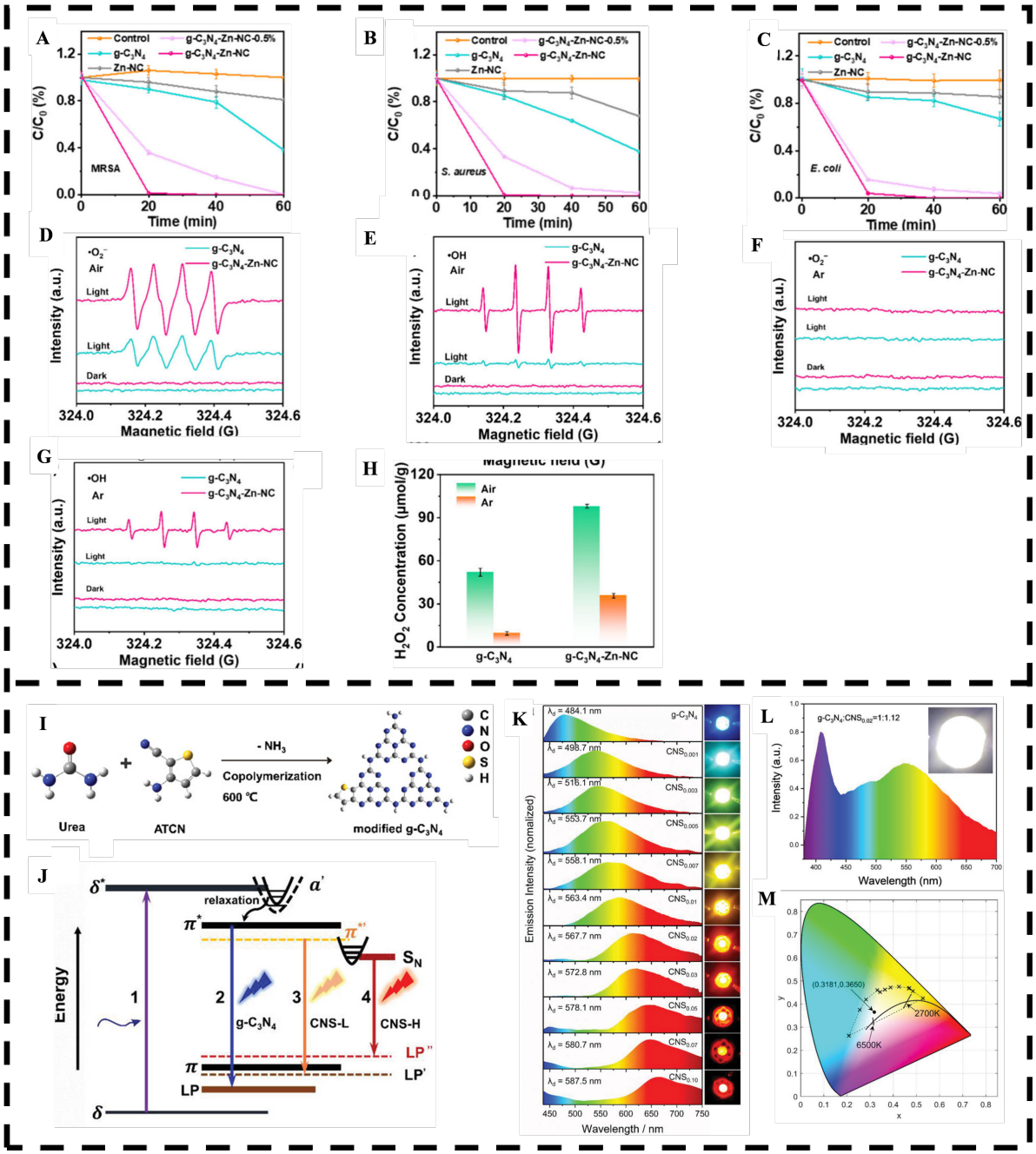

Figure 9. (A) MRSA, (B) S. aureus, and (C) E. coli under different irradiation times. Generation of (D ,F) $\cdot O_2^-$ and (E,G) ·OH as determined by ESR spectra under air and Ar. (H) H_2O_2 generation by g-C_3N_4 and g-C_3N_4–Z. *Copyright © 2024, American Chemical Society*. (I) Proposed molecular structure of g-C_3N_4 modified by 2-aminothiophene-3-carbonitrile.n-NC under air and Ar. (J) hematic energy level diagram of the PL emission of multicolor g-CN samples. (K) Emission spectra of various modified g-C_3N_4-based LEDs and photograph of the working devices. (L) Emission spectrum and photograph of a white-light LED that was produced by mixing the light from g-C_3N_4 and CNS0.02 with a weighting of 1:1.12. (M) Gamut enclosed by the chromaticities of the various LEDs, the chromaticity region of typical white light for general illumination (i.e., CCT between 2700 and 6500 K; Duv between -0.01 and +0.01), and the chromaticities of the white light. *© 2019 WILEY-VCH Verlag GmbH & Co. KGaA, Weinheim.*

radiative recombination pathways. Guo et al. [82] constructed an energy-level evolution model for multicolor emission (Figure 9(J)) by chemically regulating the ratio of $\pi \rightarrow \pi^*$ and $n \rightarrow \pi^*$ transitions within g-C_3N_4 molecular junctions (Figure 9(I)). By precisely controlling the chemical environment of the molecular junctions, the researchers successfully achieved full-spectrum coverage of the material's luminescence from blue to red (Figure 9(K)). Various modified g-C_3N_4-based LED devices fabricated on this principle exhibit excellent spectral stability. By blending g-C_3N_4 with $CNS_{0.02}$ at specific ratios,

white-light LEDs with exceptional color purity were successfully prepared (Figure 9(L)).

Chromaticity coordinate analysis (Figure 9(M)) indicates that this series of devices covers a wide range of correlated color temperatures (2700–6500 K), with color rendering characteristics that perfectly align with general lighting standards. This achievement not only reveals the bridging role of molecular junction engineering between photocatalysis and optoelectronics but also opens a new avenue for developing low-cost, sustainable organic optoelectronic devices.

5 Conclusion

This review systematically highlights a paradigm shift in the design of graphitic carbon nitride (g-C_3N_4 photocatalysts: transitioning from traditional "band structure engineering" toward atomic-level "electric field engineering." We elucidate how molecular junctions—categorized into homojunctions and heterojunctions—function as intrinsic rectifiers for charge carriers. The core achievement of this strategy lies in the induction of robust BIEF, which provide the essential thermodynamic driving force to overcome high exciton binding energies and achieve the spatial isolation of redox centers. As demonstrated in applications ranging from solar-driven hydrogen production to selective chemical synthesis, the construction of molecular junctions fundamentally transforms the random diffusion of excitons into directed migration, offering a definitive pathway to resolve the kinetic bottlenecks inherent in polymeric semiconductors.

Despite these advances, the precise experimental quantification of BIEF in g-C_3N_4-based systems remains a critical challenge. Current characterization techniques, such as KPFM, SPV, and ultrafast transient spectroscopy, primarily provide indirect or semi-quantitative insights into charge redistribution and carrier dynamics, rather than direct measurements of electric field strength. The lack of methodologies capable of simultaneously resolving the magnitude, spatial distribution, and ultrafast evolution of BIEF at the molecular scale significantly limits a deeper mechanistic understanding of electric field-driven charge separation. Therefore, future efforts should place a premium not only on atomically precise synthetic protocols, but also on the development of advanced operando and multimodal characterization techniques with high spatial and temporal resolution, which are essential for transforming electric field engineering from a conceptual framework into a quantitatively controllable strategy.

Data Availability Statement

Not applicable.

Funding

This work was financially supported by the Natural Science Foundation of Jiangsu Province, China under Grant BK20240332, and the Big Data Computing Center of Southeast University, China.

Conflicts of Interest

The authors declare no conflicts of interest.

AI Use Statement

The authors declare that no generative AI was used in the preparation of this manuscript.

Ethical Approval and Consent to Participate

Not applicable.

References

[1] Wang, X., Maeda, K., Thomas, A., Takanabe, K., Xin, G., Carlsson, J. M., Domen, K., & Antonietti, M. (2009). A metal-free polymeric photocatalyst for hydrogen production from water under visible light. *Nature Materials, 8*(1), 76-80. [CrossRef]

[2] Babu, P., Park, H., & Park, J. Y. (2023). Surface chemistry of graphitic carbon nitride: doping and plasmonic effect, and photocatalytic applications. *Surface Science and Technology, 1*(1), 29. [CrossRef]

[3] Lu, X. J., Ullah, I., Li, J. H., Chen, S., Yuan, C. Z., & Xu, A. W. (2024). A bimetallic CoZn metal–organic-framework derived CoZnS@NSC co-catalyst loaded on g-C_3N_4 for significantly augmented photocatalytic H_2 evolution. *Inorganic Chemistry Frontiers, 11*(12), 3435-3445. [CrossRef]

[4] Kumar, P., Laishram, D., Sharma, R. K., Vinu, A., Hu, J., & Kibria, M. G. (2021). Boosting photocatalytic activity using carbon nitride based 2D/2D van der Waals heterojunctions. *Chemistry of Materials, 33*(23), 9012-9092. [CrossRef]

[5] Gunawan, D., Zhang, J., Li, Q., Toe, C. Y., Scott, J., Antonietti, M., ... & Amal, R. (2024). Materials advances in photocatalytic solar hydrogen production: integrating systems and economics for a sustainable future. *Advanced Materials, 36*(42), 2404618. [CrossRef]

[6] Ruan, X., Huang, C., Cheng, H., Zhang, Z., Cui, Y., Li, Z., ... & Yu, J. (2023). A twin S-scheme

artificial photosynthetic system with self-assembled heterojunctions yields superior photocatalytic hydrogen evolution rate. *Advanced Materials, 35*(6), 2209141. [CrossRef]

[7] Panchal, P., Sharma, R., Reddy, A. S., Nehra, K., Sharma, A., & Nehra, S. P. (2023). Eco-friendly synthesis of Ag-doped ZnO/MgO as a potential photocatalyst for antimicrobial and dye degradation applications. *Coordination Chemistry Reviews, 493*, 215283. [CrossRef]

[8] Li, Z., Gao, T., Chu, H., Liao, L., Wang, X., Guo, L., ... & Zhou, W. (2024). Unraveling the nature of local field distortion-induced dual electron-trapping centers for efficient photocatalytic fuel evolution. *Applied Catalysis B: Environment and Energy, 358*, 124370. [CrossRef]

[9] Zhang, L., Li, R. H., Li, X. X., Wang, S., Liu, J., Hong, X. X., ... & Lan, Y. Q. (2024). Photocatalytic aerobic oxidation of C(sp^3)-H bonds. *Nature Communications, 15*(1), 537. [CrossRef]

[10] Luo, Z., Ye, X., Zhang, S., Xue, S., Yang, C., Hou, Y., ... & Wang, X. (2022). Unveiling the charge transfer dynamics steered by built-in electric fields in BiOBr photocatalysts. *Nature Communications, 13*(1), 2230. [CrossRef]

[11] Low, J., Yu, J., Jaroniec, M., Wageh, S., & Al-Ghamdi, A. A. (2017). Heterojunction photocatalysts. *Advanced materials, 29*(20), 1601694. [CrossRef]

[12] Wang, H., Zhang, L., Chen, Z., Hu, J., Li, S., Wang, Z., ... & Wang, X. (2014). Semiconductor heterojunction photocatalysts: design, construction, and photocatalytic performances. *Chemical Society Reviews, 43*(15), 5234-5244. [CrossRef]

[13] Liu, J., Jin, L., Dai, Z., Ji, Y., Qian, J., Lu, Y., ... & Zhai, J. (2025). Single atom embedding enhanced macroscopic polarization in carbon nitride nanosheets for pH-universal Piezo-photocatalytic nitrate reduction over a wide concentration range. *ACS Catalysis, 15*(5), 4025-4038. [CrossRef]

[14] Bi, F., Su, Y., Zhang, Y., Chen, M., Darr, J. A., Weng, X., & Wu, Z. (2022). Vacancy-defect semiconductor quantum dots induced an S-scheme charge transfer pathway in 0D/2D structures under visible-light irradiation. *Applied Catalysis B: Environmental, 306*, 121109. [CrossRef]

[15] Kofuji, Y., Ohkita, S., Shiraishi, Y., Sakamoto, H., Tanaka, S., Ichikawa, S., & Hirai, T. (2016). Graphitic carbon nitride doped with biphenyl diimide: efficient photocatalyst for hydrogen peroxide production from water and molecular oxygen by sunlight. *Acs Catalysis, 6*(10), 7021-7029. [CrossRef]

[16] Kofuji, Y., Ohkita, S., Shiraishi, Y., Sakamoto, H., Ichikawa, S., Tanaka, S., & Hirai, T. (2017). Mellitic triimide-doped carbon nitride as sunlight-driven photocatalysts for hydrogen peroxide production. *ACS Sustainable Chemistry & Engineering, 5*(8), 6478-6485. [CrossRef]

[17] Kofuji, Y., Isobe, Y., Shiraishi, Y., Sakamoto, H., Ichikawa, S., Tanaka, S., & Hirai, T. (2018). Hydrogen peroxide production on a carbon nitride–boron nitride-reduced graphene oxide hybrid photocatalyst under visible light. *ChemCatChem, 10*(9), 2070-2077. [CrossRef]

[18] Fang, X., Gao, R., Yang, Y., & Yan, D. (2019). A cocrystal precursor strategy for carbon-rich graphitic carbon nitride toward high-efficiency photocatalytic overall water splitting. *Iscience, 16*, 22-30. [CrossRef]

[19] Pan, Z., Niu, P., Liu, M., Zhang, G., Zhu, Z., & Wang, X. (2020). Molecular junctions on polymeric carbon nitrides with enhanced photocatalytic performance. *ChemSusChem, 13*(5), 888-892. [CrossRef]

[20] Pan, Z., Liu, M., Zhang, G., Zhuzhang, H., & Wang, X. (2021). Molecular triazine–heptazine junctions promoting exciton dissociation for overall water splitting with visible light. *The Journal of Physical Chemistry C, 125*(18), 9818-9826. [CrossRef]

[21] Li, Y., Jiang, Z., Dong, G., & Ho, W. (2022). Construction and Activity of an All-Organic Heterojunction Photocatalyst Based on Melem and Pyromellitic Dianhydride. *ChemSusChem, 15*(12), e202200477. [CrossRef]

[22] Chang, J. N., Li, Q., Shi, J. W., Zhang, M., Zhang, L., Li, S., ... & Lan, Y. Q. (2023). Oxidation-reduction molecular junction covalent organic frameworks for full reaction photosynthesis of H_2O_2. *Angewandte Chemie, 135*(9), e202218868. [CrossRef]

[23] Yang, M. Y., Zhang, S. B., Zhang, M., Li, Z. H., Liu, Y. F., Liao, X., ... & Lan, Y. Q. (2024). Three-motif molecular junction type covalent organic frameworks for efficient photocatalytic aerobic oxidation. *Journal of the American Chemical Society, 146*(5), 3396-3404. [CrossRef]

[24] Xiao, T., Li, K., Tang, J., Xu, Y., Li, Z., Du, R., ... & Wu, M. (2025). Achieving Efficient Solar Hydrogen Production via a Three-Motif Molecular Junction with Spatially Separated Dual Reduction Sites. *ACS nano, 19*(36), 32891-32908. [CrossRef]

[25] Yan, Y., Zhou, T., Liu, C., Hu, B., & Che, G. (2025). Dual-pathway photosynthesis H_2O_2 realized by carbon nitride with strong built-in electric field and awakened n-π^* electron transition: Based on theoretical calculation guidance. *Chemical Engineering Journal, 516*, 164108. [CrossRef]

[26] Yang, H., Sun, S., Yang, Q., Chen, A., & Cui, J. (2025). Emerging In-Plane Junctions in Graphitic Carbon Nitride for Remarkably Enhanced Photocatalysis. *Advanced Functional Materials, 35*(52), e10882. [CrossRef]

[27] Zhao, D., Wang, Y., Dong, C. L., Meng, F., Huang, Y. C., Zhang, Q., ... & Shen, S. (2022). Electron-deficient Zn-N6 configuration enabling polymeric carbon nitride for visible-light photocatalytic overall water splitting. *Nano-Micro Letters, 14*(1), 223. [CrossRef]

[28] Lin, J., Tian, W., Zhang, H., Sun, H., & Wang, S. (2024).

Electronic structure and functions of carbon nitride in frontier green catalysis. *Accounts of chemical research, 57*(16), 2303-2315. [CrossRef]

[29] Pei, J., Li, H., Yu, D., & Zhang, D. (2024). g-C_3N_4-based heterojunction for enhanced photocatalytic performance: A review of fabrications, applications, and perspectives. *Catalysts, 14*(11), 825. [CrossRef]

[30] Li, Y., Zhou, M., Cheng, B., & Shao, Y. (2020). Recent advances in g-C_3N_4-based heterojunction photocatalysts. *Journal of Materials Science & Technology, 56*, 1-17. [CrossRef]

[31] Che, W., Zhao, S., Byun, W. J., Tao, T., Jeon, J. P., Zhao, Q., ... & Baek, J. B. (2025). From carbon nitrides to COFs: Opportunities and prospects in photocatalytic CO_2 reduction. *Advanced Materials, 37*(45), e06961. [CrossRef]

[32] Zhang, L., Li, R. H., Li, X. X., Liu, J., Guan, W., Dong, L. Z., ... & Lan, Y. Q. (2022). Molecular oxidation-reduction junctions for artificial photosynthetic overall reaction. *Proceedings of the National Academy of Sciences, 119*(40), e2210550119. [CrossRef]

[33] Liang, H., Xu, Q., Cheng, R., Jing, S., Chen, F., & Tsiakaras, P. (2025). Triggering n $\rightarrow \pi^*$ electronic transitions by thiazole modified graphitic carbon nitride for enhanced photocatalytic hydrogen peroxide production and Rhodamine B degradation. *Carbon*, 120603. [CrossRef]

[34] Ye, Q., Yang, R., Huang, L., Li, Q., Zhang, Q., Li, D., ... & Jiang, D. (2023). Bridging engineering of polymeric carbon nitride for boosting photocatalytic CO_2 reduction. *Journal of Colloid and Interface Science, 652*, 813-824. [CrossRef]

[35] Li, J., Zhang, H., Li, Y., Wu, S., Wei, S., Zhang, F., ... & Xiao, H. (2025). Asymmetrical intra-molecular junction enables redox active sites on bio-decorated carbon nitride toward H_2O_2 photosynthesis. *Chemical Engineering Journal, 519*, 165018. [CrossRef]

[36] Li, K., Xiao, T., Tang, J., Du, R., Tu, J., Xie, F., ... & Wu, M. (2025). Synergetic non-covalent and covalent functionalization of carbon nitride with donor-acceptor molecules for enhanced photocatalytic hydrogen evolution performance. *Applied Catalysis B: Environment and Energy, 371*, 125201. [CrossRef]

[37] Nesaragi, A. R., Dongre, S., Iqbal, A., Thapa, R., Balakrishna, R. G., & Patil, S. A. (2025). Graphitic-carbon nitride immobilized Schiff base Palladium (II): Highly efficient electrocatalyst for hydrogen evolution reaction and density functional theory calculations. *International Journal of Hydrogen Energy, 117*, 314-324. [CrossRef]

[38] Zhou, J., Li, J., Kan, L., Zhang, L., Huang, Q., Yan, Y., ... & Lan, Y. Q. (2022). Linking oxidative and reductive clusters to prepare crystalline porous catalysts for photocatalytic CO_2 reduction with H_2O. *Nature Communications, 13*(1), 4681. [CrossRef]

[39] Yang, J., Wu, Z., He, B., & She, W. (2026). Superhydrophobic Surface for Ice Mitigation: Mechanisms, Fabrication Strategies, and Applications. *Journal of Advanced Materials Research, 2*(1), 14-39. [CrossRef]

[40] Li, J. L., Deng, X. Y., Chen, J., Fu, P. X., Tian, S. Y., Wang, Y., ... & Lei, T. (2025). Cationic conjugated polymers with enhanced doped-state planarity for n-type organic thermoelectrics. *CCS Chemistry, 7*(5), 1449-1458. [CrossRef]

[41] Bisquert, J. (2002). Theory of the impedance of electron diffusion and recombination in a thin layer. *The Journal of Physical Chemistry B, 106*(2), 325-333. [CrossRef]

[42] Li, Y., Gong, F., Zhou, Q., Feng, X., Fan, J., & Xiang, Q. (2020). Crystalline isotype heptazine-/triazine-based carbon nitride heterojunctions for an improved hydrogen evolution. *Applied Catalysis B: Environmental, 268*, 118381. [CrossRef]

[43] Ruan, X., Cui, X., Jia, G., Wu, J., Zhao, J., Singh, D. J., ... & Zheng, W. (2022). Intramolecular heterostructured carbon nitride with heptazine-triazine for enhanced photocatalytic hydrogen evolution. *Chemical Engineering Journal, 428*, 132579. [CrossRef]

[44] Chen, X., Li, X., Wu, J., Fang, C., Ding, J., Wan, H., & Guan, G. (2022). Boosting photocatalytic H_2 evolution by ingenious construction of isotype heptazine/triazine based porous carbon nitride heterojunction. *Separation and Purification Technology, 297*, 121490. [CrossRef]

[45] Yang, J., Liang, Y., Li, K., Yang, G., Wang, K., Xu, R., & Xie, X. (2020). One-step synthesis of novel K+ and cyano groups decorated triazine-/heptazine-based g-C3N4 tubular homojunctions for boosting photocatalytic H2 evolution. *Applied Catalysis B: Environmental, 262*, 118252. [CrossRef]

[46] Xia, J., Mark, G., Tong, Y., Hu, T., Volokh, M., Han, F., ... & Shalom, M. (2024). Enhancing the Activity of a Carbon Nitride Photocatalyst by Constructing a Triazine–Heptazine Homojunction. *Inorganic Chemistry, 63*(21), 10050-10056. [CrossRef]

[47] Zhang, Y., Cao, Q., Meng, A., Wu, X., Xiao, Y., Su, C., & Zhang, Q. (2023). Molecular heptazine–triazine junction over carbon nitride frameworks for artificial photosynthesis of hydrogen peroxide. *Advanced Materials, 35*(48), 2306831. [CrossRef]

[48] Han, S. G., Zhang, M., Fu, Z. H., Zheng, L., Ma, D. D., Wu, X. T., & Zhu, Q. L. (2022). Enzyme-inspired microenvironment engineering of a single-molecular heterojunction for promoting concerted electrochemical CO_2 reduction. *Advanced Materials, 34*(34), 2202830. [CrossRef]

[49] Roncali, J. (2009). Molecular bulk heterojunctions: An emerging approach to organic solar cells. *Accounts of Chemical Research, 42*(11), 1719-1730. [CrossRef]

[50] Li, L., Zhou, Z., Shi, Y., Tang, R., Li, W., Deng, Y., & Huang, Y. (2025). Donor–acceptor type carbon nitride photocatalysts in photocatalysis: current understanding, applications and challenges. *Small, 21*(8), 2409903. [CrossRef]

[51] Yang, C., Wan, S., Zhu, B., Yu, J., & Cao, S. (2022). Calcination-regulated microstructures of donor-acceptor polymers towards enhanced and stable photocatalytic H_2O_2 production in pure water. *Angewandte Chemie International Edition, 61*(39), e202208438. [CrossRef]

[52] Wang, L., Liu, L., Li, Y., Xu, Y., Nie, W., Cheng, Z., ... & Fan, Z. (2024). Molecular-level regulation strategies toward efficient charge separation in donor-acceptor type conjugated polymers for boosted energy-related photocatalysis. *Advanced Energy Materials, 14*(5), 2303346. [CrossRef]

[53] Hu, Y., Zhang, S., Zhang, Z., Zhou, H., Li, B., Sun, Z., ... & Wang, S. (2023). Enhancing photocatalytic-transfer semi-hydrogenation of alkynes over Pd/C_3N_4 through dual regulation of nitrogen defects and the Mott–Schottky effect. *Advanced Materials, 35*(41), 2304130. [CrossRef]

[54] Rao, S., Lu, Z., Xie, J., Li, Z., Liu, H., Yu, X., ... & Yang, J. (2024). Atomic Zn–N_4 site-regulated donor–acceptor catalyst for boosting photocatalytic bactericidal activity. *Nano Letters, 24*(49), 15598-15606. [CrossRef]

[55] Xie, Z. K., Jia, Y. J., Huang, Y. Y., Xu, D. B., Wu, X. J., Chen, M., & Shi, W. D. (2023). Near-infrared light-driven photocatalytic reforming lignocellulose into H2 and chemicals over heterogeneous carbon nitride. *ACS Catalysis, 13*(20), 13768-13776. [CrossRef]

[56] Zhang, Z., Ren, L., Li, H., Jiang, D., Fang, Y., Du, H., ... & Yuan, Y. (2023). π-conjugated in-plane heterostructure enables long-lived shallow trapping in graphitic carbon nitride for increased photocatalytic hydrogen generation. *Small, 19*(18), 2207173. [CrossRef]

[57] Jia, G., Wang, Y., Cui, X., Yang, Z., Liu, L., Zhang, H., ... & Zheng, W. (2019). Asymmetric embedded benzene ring enhances charge transfer of carbon nitride for photocatalytic hydrogen generation. *Applied Catalysis B: Environmental, 258*, 117959. [CrossRef]

[58] Shan, T., Wang, Y., Luo, D., Huang, Z., Zhang, F., Wu, H., ... & Xiao, H. (2024). Extended H-bonds/π-bonds networks for boosting electron transfer over polydopamine-covered nanocellulose/g-C_3N_4 toward efficient photocatalytic H_2O_2 production. *Applied Catalysis B: Environment and Energy, 349*, 123872. [CrossRef]

[59] Shan, T., Li, J., Wu, S., Wu, H., Zhang, F., Liao, G., ... & Chen, L. (2023). Boosting H_2O_2 production over carboxymethyl cellulose modified g-C_3N_4 via hydrogen-bonding-assisted charge transfer. *Chemical Engineering Journal, 478*, 147509. [CrossRef]

[60] Li, J., Zhan, G., Yu, Y., & Zhang, L. (2016). Superior visible light hydrogen evolution of Janus bilayer junctions via atomic-level charge flow steering. *Nature Communications, 7*(1), 11480. [CrossRef]

[61] Ruan, Q., Miao, T., Wang, H., & Tang, J. (2020). Insight on shallow trap states-introduced photocathodic performance in n-type polymer photocatalysts. *Journal of the American Chemical Society, 142*(6), 2795-2802. [CrossRef]

[62] Kosco, J., Gonzalez-Carrero, S., Howells, C. T., Fei, T., Dong, Y., Sougrat, R., ... & McCulloch, I. (2022). Generation of long-lived charges in organic semiconductor heterojunction nanoparticles for efficient photocatalytic hydrogen evolution. *Nature Energy, 7*(4), 340-351. [CrossRef]

[63] Godin, R., Wang, Y., Zwijnenburg, M. A., Tang, J., & Durrant, J. R. (2017). Time-resolved spectroscopic investigation of charge trapping in carbon nitrides photocatalysts for hydrogen generation. *Journal of the American Chemical Society, 139*(14), 5216-5224. [CrossRef]

[64] Lin, H., Wang, J., Zhao, J., Zhuang, Y., Liu, B., Zhu, Y., ... & Long, J. (2022). Molecular dipole-induced photoredox catalysis for hydrogen evolution over self-assembled naphthalimide nanoribbons. *Angewandte Chemie International Edition, 61*(12), e202117645. [CrossRef]

[65] Corp, K. L., & Schlenker, C. W. (2017). Ultrafast spectroscopy reveals electron-transfer cascade that improves hydrogen evolution with carbon nitride photocatalysts. *Journal of the American Chemical Society, 139*(23), 7904-7912. [CrossRef]

[66] Zhang, P., Sun, D., Cho, A., Weon, S., Lee, S., Lee, J., ... & Choi, W. (2019). Modified carbon nitride nanozyme as bifunctional glucose oxidase-peroxidase for metal-free bioinspired cascade photocatalysis. *Nature communications, 10*(1), 940. [CrossRef]

[67] Bahruji, H., Bowker, M., Davies, P. R., Al-Mazroai, L. S., Dickinson, A., Greaves, J., ... & Pedrono, F. (2010). Sustainable H_2 gas production by photocatalysis. *Journal of Photochemistry and Photobiology A: Chemistry, 216*(2-3), 115-118. [CrossRef]

[68] Frei, H. (2017). Photocatalytic fuel production. *Current Opinion in Electrochemistry, 2*(1), 128-135. [CrossRef]

[69] Nishioka, S., Osterloh, F. E., Wang, X., Mallouk, T. E., & Maeda, K. (2023). Photocatalytic water splitting. *Nature Reviews Methods Primers, 3*(1), 42. [CrossRef]

[70] Villa, K., Galán-Mascarós, J. R., López, N., & Palomares, E. (2021). Photocatalytic water splitting: advantages and challenges. *Sustainable Energy & Fuels, 5*(18), 4560-4569. [CrossRef]

[71] Hu, W., Lin, L., Zhang, R., Yang, C., & Yang, J. (2017). Highly efficient photocatalytic water splitting over edge-modified phosphorene nanoribbons. *Journal of the American Chemical Society, 139*(43), 15429-15436. [CrossRef]

[72] Shu, C., Yang, X., Liu, L., Hu, X., Sun, R., Yang, X., ... & Wang, X. (2024). Mixed-linker strategy for the construction of sulfone-containing D–A–A covalent organic frameworks for efficient photocatalytic hydrogen peroxide production. *Angewandte Chemie International Edition*, *63*(22), e202403926. [CrossRef]

[73] Nie, L., Chen, H., Wang, J., Yang, Y., & Fang, C. (2024). Enhanced visible-light H_2O_2 production over Pt/g-C3N4 Schottky junction photocatalyst. *Inorganic Chemistry*, *63*(10), 4770-4782. [CrossRef]

[74] Wang, L., Sun, J., Cheng, B., He, R., & Yu, J. (2023). S-scheme heterojunction photocatalysts for H_2O_2 production. *The Journal of Physical Chemistry Letters*, *14*(20), 4803-4814. [CrossRef]

[75] Zhao, J., Wang, L., Zhou, T., Yan, Y., Sun, J., Hu, B., ... & Che, G. (2025). Molecularly tunable donor–acceptor integrated carbon nitride for sunlight-driven H_2O_2 synthesis: Mechanism and performance insights. *Small*, *21*(17), 2500679. [CrossRef]

[76] Windle, C. D., & Perutz, R. N. (2012). Advances in molecular photocatalytic and electrocatalytic CO_2 reduction. *Coordination Chemistry Reviews*, *256*(21-22), 2562–2570. [CrossRef]

[77] Xie, W., Ce, M., Chen, T., Liu, X. H., Yan, H., Zhang, X., ... & Huang, H. (2026). Reversing V=O orientation of vanadyl phthalocyanine as "molecular switch" on carbon nitride boosts CO_2 photoreduction. *Angewandte Chemie*, e23201. [CrossRef]

[78] Nosaka, Y., & Nosaka, A. Y. (2017). Generation and detection of reactive oxygen species in photocatalysis. *Chemical Reviews*, *117*(17), 11302-11336. [CrossRef]

[79] Wang, D., Chen, S., Lai, S., Dai, W., Yang, L., Deng, L., ... & Luo, S. L. (2023). Advanced municipal wastewater treatment and simultaneous energy/resource recovery via photo (electro) catalysis. *Chinese Chemical Letters*, *34*(5), 107861. [CrossRef]

[80] Ran, B., Ran, L., Wang, Z., Liao, J., Li, D., Chen, K., ... & Peng, X. (2023). Photocatalytic antimicrobials: principles, design strategies, and applications. *Chemical reviews*, *123*(22), 12371-12430. [CrossRef]

[81] Li, H., Cheng, Z., Zhou, Z., Hu, C., Ye, J., Huang, D., ... & Li, J. (2026). High Luminous Efficacy and Thermal Stability of LuAG: Ce Phosphor Ceramics with Porosity for High-brightness Laser Lighting. *Journal of Advanced Materials Research*, *2*(2), 86-96. [CrossRef]

[82] Guo, Q., Wei, M., Zheng, Z., Huang, X., Song, X., Qiu, S. B., ... & Dong, G. (2019). Full-color chemically modulated g-C_3N_4 for white-light-emitting device. *Advanced Optical Materials*, *7*(21), 1900775. [CrossRef]

Kaichi Chen received the B.S. degree in material science and engineering from Southeast University, Nanjing 211189, China, in 2024. (Email: 220246857@seu.edu.cn)

Zhicheng Zheng received the B.S. degree in material science and engineering from Fuzhou University, Fuzhou 350108, China, in 2024. (Email: 220242761@seu.edu.cn)

Yukun Fang Currently studying for a master's degree in materials science and engineering from Southeast University, Nanjing 211189, China. (Email: 220242666@seu.edu.cn)

Yuanyuan Liu received her Ph.D. from Southeast University in 2021. Currently, she is a lecturer in the School of Materials and Chemical Engineering at the Xuzhou University of Technology. She mainly focuses on the synthesis and application of functional materials, such as photocatalysis, biosensor, and supercapacitors. (Email: liuyuanyuan@xzit.edu.cn)

Xinli Guo currently working at Southeast University in China as a full professor. He has worked at various research and academic institutions, including the Nanxi Mining Institute in France, the University of Seoul in South Korea, the National Institute of Materials Research (NIMS) in Japan, and the University of Osaka. He focuses on semiconductor nano-photocatalytic materials for energy conversion/storage systems. (Email: guo.xinli@seu.edu.cn)